An-Najah National University

Faculty of Graduate Studies

STRUCTURAL, ELECTRONIC, MAGNETIC, AND ELASTIC PROPERTIES OF THE FULL-HEUSLER COMPOUNDS: Co_2MnSi, Co_2MnGe USING FP-LAPW METHOD

By

Duaa Ali Mohammad Hasan

Supervisors

Dr. Mahmoud Farout

Prof. Mohammed Abu-Jafar

This Thesis is Submitted in Partial Fulfillment of the Requirements for the Degree of Master of Physics, Faculty of Graduate Studies, An-Najah National University, Nablus, Palestine.

2025

STRUCTURAL, ELECTRONIC, MAGNETIC, AND ELASTIC PROPERTIES OF THE FULL-HEUSLER COMPOUNDS: Co_2MnSi, Co_2MnGe USING FP-LAPW METHOD

By
Duaa Ali Mohammad Hasan

This Thesis was Defended Successfully on 13/02/2025 and approved by

Dr. Mahmoud Farout	
Supervisor	Signature
Prof. Mohammed Abu-Jafar	
Co-Supervisor	Signature
Dr. Noorhan Alshaikh Mohammad	
External Examiner	Signature
Dr. Khaled Ilaiwi	
Internal Examiner	Signature

Dedication

I'm highly grateful to my beloved family. To my beloved parents for all the sacrifices they have made to make my future better. ALLAH bless them. To my lovely brothers and sisters who always encourage me and give me powerful support.

Acknowledgments

All thanks to Allah, who gives me health, knowledge and patience to complete my thesis. I would like to acknowledge the following people who helped me in many aspects that made me possible to write this thesis. At first, I address a special thanks to my supervisor and instructor Dr. Mahmoud Farout for his continuous support, effortless helps, valuable discussions and humble guidance. I also thank my co-supervisor and instructor Prof. Dr. Mohammed Abu-Jafar for everything he did to help me complete this study. They always encourage my work and allow me to think and execute my plans independently. I really feel so lucky to have them as my supervisors. Never forget my faculty members of physics department for their help and encouragement.

Declaration

I, the undersigned, declare that I submitted the thesis entitled:

STRUCTURAL, ELECTRONIC, MAGNETIC, AND ELASTIC PROPERTIES OF THE FULL-HEUSLER COMPOUNDS: Co_2MnSi, Co_2MnGe USING FP-LAPW METHOD

I declare that the work provided in this thesis, unless otherwise referenced, is the researcher's own work, and has not been submitted elsewhere for any other degree or qualification.

Student's Name: Duaa Ali Mohammad Hasan.

Signature: Duaa

Date: 13-2-2025.

List of Contents

Dedication iii
Acknowledgments iv
Declaration v
List of Contents vi
List of Tables vii
List of Figures viii
List of Appendices ix
Abstract x
Chapter One: Introduction 1
Chapter Two: Methodology 12
2.1 The Born-Oppenheimer Approximation (BOA) 12
2.2 Hartree and Hartree-Fock Approximation 13
2.3 Density Functional Theory (DFT) 13
2.4 Single particle Kohn-Sham Equation 14
2.5 The Exchange-Correlation Functional 17
2.6 Local Density Approximation (LDA) 17
2.7 Generalized Gradient Approximation (GGA) 18
2.8 Augmented Plane Wave (APW) Method 18
2.9 The Linearized Augmented Plane Wave (LAPW) Method 19
2.10 Modified Becke-Johnson Potential (mBJ) 20
Chapter Three: Results and Discussion 21
3.1 Computational Method 21
3.2 Structural Properties 22
3.3 Magnetic Properties 26
3.4 Electronic Properties 31
3.5 Elastic Properties 43
Chapter Four: Discussions and Conclusions 47
List of Abbreviations 50
References 51
Appendices 56
الملخص ..... ب

List of Tables

Table 1: Calculated lattice parameter (a), bulk modulus (B), first pressure derivative of the Bulk modulus (B') and minimum energy E0 for normal and inverse Heusler Co_2MnSi and Co_2MnGe Heusler compounds 25

Table 2: Total, atomic and interstitial GGA magnetic moment of normal and inverse Heusler compounds Co_2MnZ where Z (Si. Ge) 28

Table 3: Total, atomic and interstitial mBJ magnetic moment for normal and inverse Heusler compounds Co_2MnZ where Z (Si. Ge) 29

Table 4: Band gap of normal and inverse Heusler compounds Co_2MnSi and Co_2MnGe 32

Table 5 Elastic constants (C_{ii}) and bulk modulus (B) of normal and inverse Heusler compounds Co_2MnSi and Co_2MnGe 44

Table 6: The Shear modulus (S), Bugh ratio (B/S), Voigt Poisson's ratio (ν), Young's modulus (Y) and anisotropic factor (A) for Heusler compounds 45

List of Figures

Figure 1: Periodic table of elements forming Heusler compounds X_2YZ 2

Figure 2: Schematic representation of Husler compounds 3

Figure 3: Flow chart of the nth repitition in the self-consistent procedure to solve Hartree-Fock or Kohn-Sham equations 16

Figure 4: Scheme of Augmented Plane Wave 18

Figure 5: Crystal structures of the full Heusler Co_2MnSi and Co_2MnGe compounds (red: Co, blue: Mn, green: Si / Ge)..... 23

Figure 6: The total energy (Ry) versus volume (a.u3) of Heusler compounds..... 24

Figure 7: Band structure of normal Co_2MnSi 33

Figure 8: Band structure of inverse Co_2MnSi..... 34

Figure 9: Band structure of normal Co_2MnGe..... 35

Figure 10: Band structure of inverse Co_2MnGe 36

List of Appendices

Appendix A: DOS Figures 56

Figure 11: TDOS and PDOS of spin-up for normal Co_2MnSi compound using GGA 56

Figure 12: TDOS and PDOS of spin-down for normal Co_2MnSi compound using GGA 57

Figure 13: TDOS and PDOS of spin-up for inverse Co_2MnSi compound using GGA 58

Figure 14: TDOS and PDOS of spin-down for inverse Co_2MnSi compound using GGA 59

Figure 15: TDOS and PDOS of spin-up for normal Co_2MnGe compound using GGA 60

Figure 16: TDOS and PDOS of spin-down for normal Co_2MnGe compound using GGA 61

Figure 17: TDOS and PDOS of spin-up for inverse Co_2MnGe compound using GGA 62

Figure 18: TDOS and PDOS of spin-down for inverse Co_2MnGe compound using GGA 63

Figure 19: TDOS and PDOS of spin-up for normal Co_2MnSi compound using mBJ 64

Figure 20: TDOS and PDOS of spin-down for normal Co_2MnSi compound using mBJ 65

Figure 21: TDOS and PDOS of spin-up for inverse Co_2MnSi compound using mBJ 66

Figure 22: TDOS and PDOS of spin-down for inverse Co_2MnSi compound using mBJ 67

Figure 23: TDOS and PDOS of spin-up for normal Co_2MnGe compound using mBJ 68

Figure 24: TDOS and PDOS of spin-down for normal Co_2MnGe compound using mBJ 69

Figure 25: TDOS and PDOS of spin-up for inverse Co_2MnGe compound using mBJ 70

Figure 26: TDOS and PDOS of spin-down for inverse Co_2MnGe compound using mBJ 71

STRUCTURAL, ELECTRONIC, MAGNETIC, AND ELASTIC PROPERTIES OF THE FULL-HEUSLER COMPOUNDS: Co_2MnSi, Co_2MnGe USING FP-LAPW METHOD

By
Duaa Ali Mohammad Hasan
Supervisors
Dr. Mahmoud Farout
Prof. Mohammed Abu-Jafar

Abstract

The Structural, electronic, magnetic, and elastic properties for both normal and inverse full-Heusler compounds Co_2MnSi and Co_2MnGe were investigated by using full potential linearized augmented plane wave (FP-LAPW) method, within density functional theory (DFT) that implemented in WEIN2k package. The generalized gradient approximation (GGA) has been used to compute the structural properties such as lattice parameter (a), bulk modulus (B), it's first pressure derivative (B') and minimum energy (E_0). Moreover, electronic,magnetic and elastic properties were found using GGA. In addition to GGA, modified Becke-Johnson Potential (mBJ) was used to enhance the band structure (BS). According to the density of states (DOS) and BS, both normal Co_2MnSi and Co_2MnGe compounds have half-metallic behavior, while invers Co_2MnSi and Co_2MnGe compounds are metallic. both normal and inverse Co_2MnSi and Co_2MnGe compounds are ferromagnetic materials. The normal Co_2MnSi and Co_2MnGe compounds and inverse Co_2MnSi are mechanically stable, whereas inverse Co_2MnGe compound is mechanically unstable. According to anisotropic factor (A), normal and inverse Heusler compounds Co_2MnSi and normal Heusler compound Co_2MnGe are elastic anisotropy. Pugh ratio (B/S) indicates that both normal and inverse Heusler compounds Co_2MnSi, and normal Heusler compound Co_2MnGe are ductile. According to Poisson's ratio (ν) normal and inverse Heusler compounds Co_2MnSi and normal Heusler compound Co_2MnGe have ionic bonds.

Keywords: Full Heusler, structural, electronic, magnetic, half-metallic, stability.

Chapter One

Introduction

Since 1903, the first Heusler alloy was discovered by the German scientist Friedrich Heusler, it was Cu_2MnAl. Surprisingly, this alloy was ferromagnetic, although none of its components show magnetic behavior by themselves. Nowadays, more than a thousand Heusler alloys are known.

Heusler compounds have many applications involve spin-gapless semiconductors (SGSs), topological insulators, spintronic (1), Shape memory (2), thermoelectric (3), and superconductors (4).

Heusler compounds belong to the class of face-centered cubic (FCC) crystalline structure of intermetallic molecules which is a kind of metallic alloy that combines two or more metallic elements to form an ordered solid-state compound. They were classified mainly into two groups, ternary and quaternary compounds (5).

Ternary Heusler compounds were divided into two groups, the first one is full Heusler compounds with chemical structure X_2YZ (2:1:1) -$L2_1$ structure, the second is half Heusler compounds with chemical structure XYZ (1:1:1) -$C1_b$ structure.

Quaternary Heusler compounds have a chemical structure XX'YZ (1:1:1:1). Where X and Y are transition metals and Z is the primary group element (5). The elements forming Heusler compounds have been indicated in figure 1 (6).

Figure 1

Periodic table of elements forming Heusler compounds X_2YZ

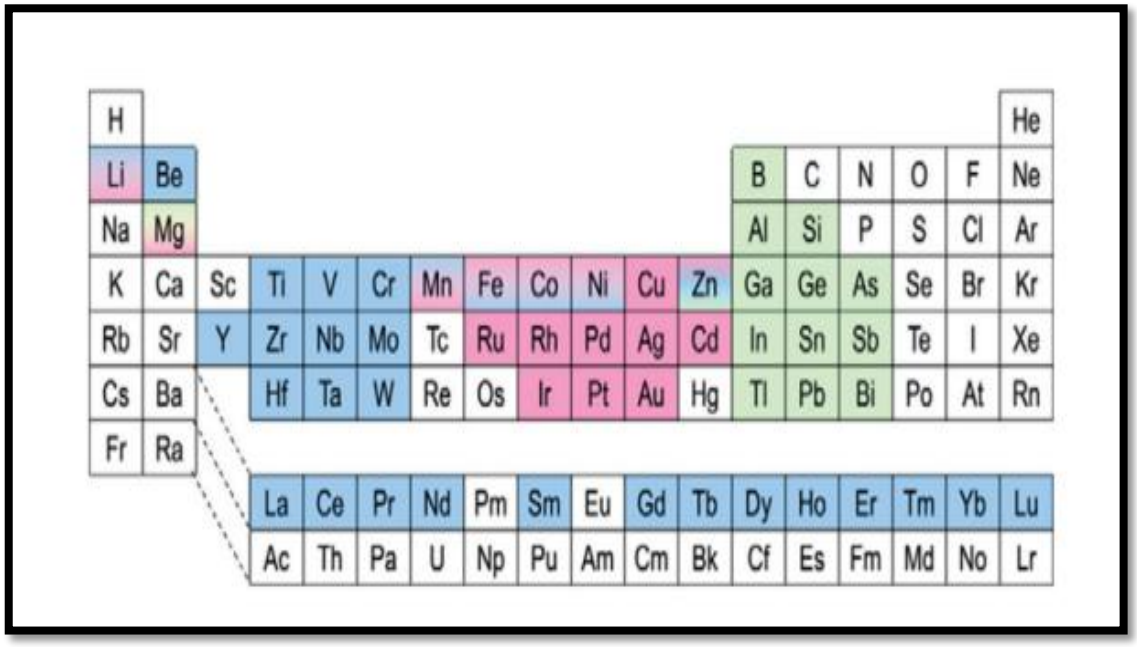

Full Heusler compounds can crystallize in two types, regular full Heusler alloy with space group 225-Fm3-m. at the positions (0.25,0.25,0.25), (0.75,0.75,0.75) for X atom, (0.5,0.5,0.5) for Y atom and (0,0,0) for Z atom.

The other one is inverse Heusler alloy with space group 216- F-43Mm at the positions (0.25,0.25,0.25), (0.5,0.5,0.5) for X atom, (0.75,0.75,0.75) for Y atom and (0,0,0) for Z atom (7).

The site of the second X atom is vacant in Half-Heusler compounds (8) – atoms at the positions (0.25,0.25,0.25) for X atom, (0.5,0.5,0.5) for Y atom and (0,0,0) for Z atom. The unit cells of $L2_1$-type and $C1_b$ have been represented in figure 2.

Figure 2

Schematic representation of Husler compounds

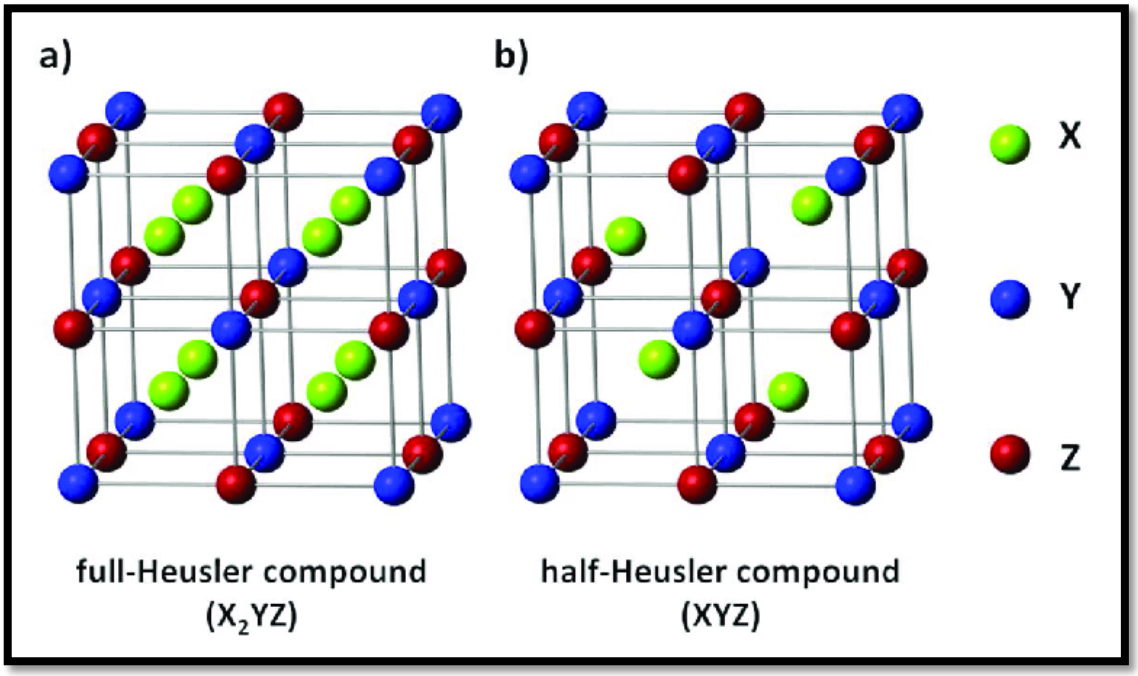

Note: (a) full Heusler and (b) half Heusler.

Some of Heusler compounds have totally different behavior for spin-up and spin-down bands. The spin-up electrons behave as metallic, whereas the spin-down electrons behave as semiconductor. These compounds called half-metallic (HM), so HM materials exhibiting a 100% spin polarization. The half-metallic materials have been proposed as a very exiting material for spintronic devices (9–18).

Heusler compounds and half-metallic compounds have been the subject of several earlier studies using various techniques.

In 1985 Brown et al (19), studied the magnetization density in Heusler alloy Fe_2MnSi by using polarized neutron diffraction and analyzed its distribution across different components of the alloy. The study investigated that that the magnetization density is unequally distributed, which reflecting the effect of the alloy's chemical structure on its magnetic properties. It's also provided a theoretical explanation of the role of Mn and Si in modifying the magnetization intensity within the alloy. In addition, it indicated the potential of Fe_2MnSi for applications requiring precise and specific magnetization because it's exhibits complex magnetic properties dependent on its chemical composition.

In 1995, Fujii et al. (20) computed the lattice constant, density of states and the band structure of Fe_2MnZ (Z=Al, Si, p) by LMTO-ASA method, to find these compounds didn't behave a half-metallic character except Fe_2MnSi. The lattice constant found to be 5.67, 5.59 and 5.56 A^0 for Fe_2MnAl, Fe_2MnSi and Fe_2MnP respectively. Fe_2MnAl atomic magnetic moment is 0.16, 2.35 and -0.03 μ_B for Fe, Mn and Al respectively. While for Fe_2MnSi it's 0.20, 2.63 and -0.04 μ_B for Fe, Mn and Si respectively. Whereas for Fe_2MnP the atomic magnetic moment is 0.66, 2.73 and -0.04 μ_B for Fe, Mn and P respectively.

Electronic and magnetic properties of Fe_2YSi (Y=Cr, Mn, Fe, Co, Ni) was found by Hongzhi et al, in 2007 (21). Lattice constant, density of state and magnetic moment was found both experimentally and theoretically.

Theoretical method they used FP-LAPW method. They found that both Fe_2CrSi and Fe_2MnSi are half-metallic ferromagnetic material. While the other compounds are metallic. The lattice constant estimated to be 5.679, 5.672, 5.654, 5.645, 5.648 and 5.648 A^0 for Fe_2CrSi, Fe_2MnSi, Fe_3Si, Fe_2CoSi, normal Fe_2NiSi and inverse Fe_2NiSi consequently. The total magnetic moment estimated to be 2 μ_B for Fe_2CrSi compound. While the atomic magnetic moment is -0.12, 2.26 and -0.02 μ_B for Fe, Cr and Si consequently. In addition, for Fe_2MnSi the total magnetic moment estimated to be 2.99 μ_B. Whereas, the atomic magnetic moment is -0.1, 3.22 and -0.02 μ_B for Fe, Mn and Si consequently. Moreover, the total magnetic moment estimated to be 5.04 μ_B for Fe_3Si compound. While the atomic magnetic moment for Fe_x, Fe_y and Si is 1.28, 2.62 and -014 μ_B consequently. Also, the total magnetic moment for Fe_2CoSi estimated to be 5 μ_B. While the atomic magnetic moment is 1.38, 2.82, 0.29 and -0.1 μ_B for Fe_1, Fe_2, Co and Si consequently. Furthermore, the total magnetic moment estimated to be 5.648 μ_B for both normal and inverse Fe_2NiSi compound. The atomic magnetic moment for normal Fe_2NiSi is 1.48, 0.4 and -0.18 μ_B for Fe, Ni and Si respectively. While the atomic magnetic moment for inverse Fe_2NiSi is 1.62, 2.58, 0.24 and -0.06 μ_B for Fe_1, Fe_2, Ni and Si respectively.

In 2007, Ishida et al, (22) had studied theoretically searched of spintronic material in two alloys systems $Fe_2(Cr_{1-x}Mn_x)Si$ and $(Fe_{1-x}Co_x)_2MnSi$ by LMTO-ASA method with LSD approximation. They found that the ferromagnetic state was stable. $Fe_2(Cr_{1-x}Mn_x)Si$ was very high spin polarized and $(Fe_{1-x}Co_x)_2MnSi$ was perfect half-metallic

material. In $(Fe_{1-x}Co_x)_2MnSi$ there were promising materials which are suitable for spintronic devices.

In 2010, Saito et al (23), studied the interface structure of a half-metallic Heusler compound Co_2MnSi thin layer when it contacts an MgO tunnelling wall by using X-ray Magnetic Circular Dichroism (XMCD). The study showed that the interface between Co_2MnSi and MgO plays an essential role in determining the magnetic and electronic properties of the film, which is very important for the application of spintronic apparatuses. It indicated that the Co_2MnSi thin film maintains its half-metallic nature, meaning it behaves as a perfect spin filter with full spin polarization at the Fermi level, which is essential for efficient spin transport. Furthermore, the study showed how the interface affects the magnetization and orbital moment of atoms at the Co_2MnSi/MgO interface.

In 2011, Itoh et al (24), studied the electronic properties and spin-injection characteristics of Co-based Heusler compounds semiconductor junctions. The study focused on understanding how the electronic structure of Co-based Heusler compounds affects their ability to inject spins into semiconductor materials, which fundamental condition for spintronics applications. The study used first principles band calculation to analyze the electronic structure of Co-based Heusler compounds, showing their semi-metallic behavior, in which the materials exhibit full spin polarization at the Fermi level. This property makes Co-based Heusler compounds promising possibilities for efficient spin injection into semiconductors, as they can inject polarized spins into the semiconductor with minimum cost.

Hamad et al, (25) in 2011 studied the impact of defects on the electronic and magnetic properties of Fe_2MnSi Heusler compound by using FP-LAPW method. They studied three defects that were antistites, swap and vacancy. Although the defects the alloy retained the half- metallicity, which means it's promising for the potential application in spintronics.

In 2012, Shigeta et al, (26) studied experimentally magnetization and spin polarization of $Co_{2-x}Fe_xMnSi$ Heusler compounds. They found that those compounds were half-metallics and the values of spin polarization (P) were less dependent on different concentrations of x. P=0.53 for x=1.25 and P=0.50 for x=0.50, respectively.

Pedro et al. (27) studied the effect of Ga replacing on the structural and magnetic characteristics of half-metallic Fe_2MnSi Heusler compound experimentally in 2015. They found that the lattice parameter has linearly increased as the increasing of Ga content in $Fe_2MnSi_{1-x}Ga_x$ Heusler compound. Moreover, the compound doesn't follow the Slater-Pauling rule, which says that "adding an element to a metal alloy will reduce the alloy's saturation magnetization by an amount proportional to the number of valence electrons outside of the added element's d shell".

In 2018, Hiroi et al. (28), studied Magnetization and magnetic phase diagram of Heusler alloys Fe_{3-} □$(Mn_{1-x}V$□)□Si (y=1 and 1.5). The study investigated experimentally the impacts of changing the Fe, Mn and V ratios on the magnetic properties at different temperature and different magnetic field. They found that there was transition phase between ferromagnetic and antiferromagnetic phase.

The magnetic characteristics of Heusler alloy $Fe_{1.3}Mn_{1.7}Si$ was studied in 2018 by Hiroi et al. (29). They found that there was transition phase between ferromagnetic and antiferromagnetic phase at different temperature.

In 2019, Arshad et al. (5), studied structural, electronic and magnetic characteristics of equiatomic quaternary CoPdCrZ (Z=Si, Ge, P) Heusler compounds theoretically. The study used full potential linearized augmented plane wave method (FP-LAPW). They study three types of alloys, type 1 with positions (0.25,0.25,0.25), (0. 5, 0. 5, 0. 5), (0.75, 0.75, 0.75) and (0, 0, 0) for Co, Pd, Cr and Z respectively. Type 2 with positions (0.25, 0.25, 0.25), (0.75, 0.75, 0.75), (0.5, 0.5 0.5) and (0, 0, 0) for Co, Pd, Cr and Z respectively. Type 3 with positions (0.5, 0.5, 0.5), (0.25, 0.25, 0.25), (0.75, 0.75, 0.75) and and (0, 0, 0) for Co, Pd, Cr and Z respectively. The lattice constant (a), bulk modulus (B) and minimum energy (E_0) for three types were found. minimum energy was indicated that the most stable type is type 2 for CoPdCrSi compound, type 2 for CoPdCrGe compound and type 1 for CoPdCrP compound The lattice constant for CoPdCrSi is 5.8317, 5.9201 and 5.8226 A^0 for type 1, type 2 and type 3 respectively. The bulk modulus is 230.9931, 186.2799 and 220.8084 GPa for type 1, type 2 and type 3 respectively. The minimum energy for type 1, type 2 and type 3 is -15562.884574, -15562.914623 and -15562.898988 eV respectively. The lattice constant for CoPdCrGe is 5.9913, 6.0222 and 5.9151 A^0 for type 1, type 2 and type 3 respectively. The bulk

modulus is 117.6941, 163.7297 and 199.2034 GPa for type 1, type 2 and type 3 respectively.

The minimum energy for type 1, type 2 and type 3 is -19180.962943, -19180.987520 and -19180.960361 eV respectively. The lattice constant for CoPdCrP is 5.8084, 5.9498 and 5.8130 A^0 for type 1, type 2 and type 3 respectively. The bulk modulus is 212.1556, 150.3140 and 209.7352 GPa for type 1, type 2 and type 3 respectively. The minimum energy for type 1, type 2 and type 3 is -15666.994232, -15666.976846 and -15666.981722 eV respectively. CoPdCrSi and CoPdCrGe have metallic behavior with zero energy gap at spin-up, but at spin-down they behave nearly half-metallically and have small energy band gap because fermi level doesn't lie in the gap. CoPdCrP behave metallically. The total magnetic moment is 4.235, 4.415 and 0.864 μ_B for CoPdCrSi, CoPdCrGe and CoPdCrP respectively.

In 2020, El Karmi et al. (30), have been studied structural, electronic, magnetic and thermoelectric characteristics of Full-Heusler Fe_2MnSi theoretically using FP-LAPW method implemented in WIEN2k. The lattice constant for normal and inverse compound is 5.5912 and 5.5911 A^0 consequently. The bulk modulus was 232.73 and 232.30 GPa for normal and inverse compound respectively. And its derivative for both normal and invers compound is 4.91 and 4.93 GPa respectively. This compound is metallic in spin-up with zero band gap, and indirect energy band gap in spin-down. Fe_2MnSi full Heusler compound is half metallic compound with 0.365 eV band gap by GGA and 0.583 eV by mBJ approximation. The total and atomic magnetic moment have calculated by both GGA and mBJ approximations, total magnetic moment is 3.0009 μ_B by GGA and 4.5079 μ_B by mBJ approximation. Partial magnetic moment for this compound by GGA is 3.0433, -0.0492, 0.0006 and 0.0555 μ_B for Mn, Fe, Si and interstitial respectively. By mBJ approximation it's 2.2169, 1.2344, -0.0532 and -0.1246 μ_B for Mn, Fe, Si and interstitial respectively. These values indicate that this compound is ferromagnetic compound.

In 2021, structural, electronic, magnetic and elastic characteristics of full Heusler compounds $Cr_{2-x}Fe_xMnSi$ have studied by Wu et al. (31), theoretically by CASTEP method. Both Cr_2MnSi and Fe_2MnSi have normal and invers structure, while CrFeMnSi have three types of structure, type 1, type 2 and type 3. The lattice constant is 5.707, 5.718, 5.579 and 5.581 A^0 for normal Cr_2MnSi, inverse Cr_2MnSi, normal Fe_2MnSi and

inverse Fe_2MnSi respectively. The lattice constant for type1, type 2 and type 3 CrFeMnSi compound is 5.709, 5.715 and 5.594 A^0 respectively. Minimum energy is -22787.5757, -22790.3715, -9972.7645 and -9971.6957 eV for normal Cr_2MnSi, inverse Cr_2MnSi, normal Fe_2MnSi and inverse Fe_2MnSi respectively. It's -16381.1621, -16379.5597 and -16382.4777 eV for type1, type2 and type 3 CrFeMnSi compound respectively. Total and atomic magnetic moment have found for all compounds. Total magnetic moment for normal Cr_2MnSi, inverse Cr_2MnSi, normal Fe_2MnSi and inverse Fe_2MnSi is 2.2, 1, 3 and 3 μ_B respectively. Total magnetic moment is 1.02, 2.24 and -1 μ_B for type1, type2 and type 3 CrFeMnSi compound respectively. Atomic magnetic moment for normal Cr_2MnSi compound is 0.62, 0.90 and 0.06 μ_B for Cr, Mn and Si respectively. While for inverse Cr_2MnSi it's 1.50, -1.44, 0.88 and 0.06 μ_B for Cr_1, Cr_2, Mn and Si respectively. In addition, for normal Fe_2MnSi the atomic magnetic moment is 0.26, 2.44 and 0.04 μ_B for Fe, Mn and Si respectively. Whereas for inverse Fe_2MnSi the atomic magnetic moment for Fe_1, Fe_2, Mn and Si is 2.24, 0.88, -0.16 and 0.04 μ_B consequently. Moreover, the atomic magnetic moment for type 1 CrFeMnSi compound is -1.76, 0.26, 2.54 and -0.02 μ_B for Cr, Fe, Mn and Si respectively. While for type 2 CrFeMnSi compound it's -1.30, 2.22, 1.48 and 0.02 μ_B for Cr, Fe, Mn and Si respectively. Whereas for type 3 CrFeMnSi compound atomic magnetic moment for Cr, Fe, Mn and Si is -1.32, -0.06, 0.38 and 0 μ_B respectively. According the band structure with density of state inverse Cr_2MnSi, normal Fe_2MnSi and type 3 CrFeMnSi compounds are half-metallic. The energy band gap is 0.136, 0.160 and 0.502 eV for Cr_2MnSi, CrFeMnSi and Fe_2MnSi consequently. These values indicate that energy band gap value increase as number of Fe atom increase in compound. The elastic constants have found to be 280.1, 155.5 and 113 GPa for C_{11}, C_{12} and C_{44} consequently for inverse Cr_2MnSi compound. Moreover it's 404.6, 156 and 137.5 GPa for C_{11}, C_{12} and C_{44} consequently for type 3 CrFeMnSi compound. In addition, the elastic constants for normal Fe_2MnSi are 307.3, 224.2 and 173.3 GPa for C_{11}, C_{12} and C_{44} consequently. All three compounds found to be mechanically stable. The bulk modulus was 197, 244.9 and 251.9 GPa for inverse Cr_2MnSi, type 3 CrFeMnSi and normal Fe_2MnSi compound respectively. Shear modulus for inverse Cr_2MnSi, type 3 CrFeMnSi and normal Fe_2MnSi compound found to be 82.4, 87.1 and 101.8 GPa respectively. Pugh's ratio found to be 2.39, 2.81 and 2.47 for inverse Cr_2MnSi, type 3 CrFeMnSi and normal Fe_2MnSi compound respectively. All three compounds found to be ductile material.

Poisson's ratio calculated for inverse Cr_2MnSi, type 3 CrFeMnSi and normal Fe_2MnSi compound to be 0.316, 0.341 and 0.322 respectively, which indicates that all three compounds are ductile. The anisotropy parameter found to be 1.18, 1.15 and 4.17 for inverse Cr_2MnSi, type 3 CrFeMnSi and normal Fe_2MnSi compound respectively. According that all three compounds are elastic anisotropic.

All previous studies mentioned above were discussed full Heusler compounds in general. There were some of studies that have specifically discussed Co_2MnSi and Co_2MnGe Heusler compounds.

In 1998, Ishida et al. (32) calculated the electric structure for Co_2MnSi and Co_2MnGe using LMTO-ASA method with LSD approximation to find them half-metallic compounds, calculated the magnetic moment and lattice parameter also. The lattice parameter for Co_2MnSi and Co_2MnGe found to be 5.620 and 5.727 A^0 consequently, the magnetic moment was 1.07 and 2.59 μ_B for Co and Mn respectively in Co_2MnSi compound, while it found to be 1.03 and 3.02 μ_B for Co and Mn respectively in Co_2MnGe compound.

In 2006, Galanakis et al. (8) calculated the magnetic moment for Co_2MnSi and Co_2MnGe from the first principles using full potential screened Korringa-Kohn-Rostoker (FSKKR) method. The total magnetic moment of these compounds was 4.940 and 4.941 μ_B respectively. The atom dependent magnetic moment for those compounds was 1.021, 2.971 and -0.047 μ_B for Co, Mn and Si respectively for for Co_2MnSi compound, on the other hand, they found to be 0.981, 3.040 and -0.061 μ_B for Co, Mn and Ge respectively for Co_2MnGe compound.

In 2015, lattice parameter for Co_2MnSi was found experimentally to be 5.661 A^0 by Bhatt et al. (33).

In 2019, Aguilera-Granja et al. (34) studied the structural, electronic, and magnetic characteristics of 60 Heusler alloys, through using SIESTA code. The lattice parameters were found to be 5.694 and 5.825 A^0 for Co_2MnSi and Co_2MnGe respectively. Both of compounds founded to be half-metallic. According to the total magnetic moment, it was 5 μ_B for both compounds. In order to partial magnetic moment, they founded to be 0.893, 3.253 and -0.037 μ_B for Co, Mn and Si atom respectively in Co_2MnSi compound.

While for Co_2MnGe compound, they founded to be 0.901, 3.395 and -0.196 μ_B for Co, Mn and Ge atom respectively. Also spin down energy gap was founded to be 0.69 and 0.58 ev for Co_2MnSi and Co_2MnGe respectively. While both compounds are metallic in spin-up with zero energy gap.

In 2021, Pradines et al. (35) used FP-LAPW method with GGA approximation to calculate lattice parameter, spin down energy gap and magnetic moment for Co_2MnSi. The lattice parameter founded to be 5.63 A^0 . the total magnetic moment was 5 μ_B. According to atom dependent magnetic moment, it was 0 1.07, 2.85 and -0.04 μ_B for Co, Mn and Si atom respectively. In order to the band gap, this compound is half-metallic. It is metallic in spin-up with zero energy gap, and semi-conductor in spin down with 0.83 ev energy gap.

All of these studies found that these two compounds have $L2_1$ structure and half-metallic ferromagnets behavior.

Importance of this study

Heusler compounds had been discovered more than a century earlier, but they attracted the researcher's attention continuously. They have amazing controllability and unuque characteristics.

Heusler alloys have a lot of exciting physical characteristics that give them the potential for a lot of applications in several technical field, including spin-gapless semiconductors (SGSs), spintronic, topological insulators, thermo-electric materials, shape memory alloys (SMAs) and superconductors.

This research is considered as a hot topic since the importance of this study lies in the totally different behavior at spin-up and spin-down bands for these materials. The spin-up electrons behave as metallic, while the spin-down electrons behave as semiconductor.

They can be categorized as metallic, semiconductors, semimetals, and various kinds of magnetic order including ferromagnets, antiferromagnets and half-metallic ferromagnets.

For spintronic and magneto-electronic applications, half-metallic magnetic materials are thought to be quite promising.

Pradines et al. (35) have been used FP-LAPW technique within generalized gradient approximation (GGA) only.

In this work modified Becke-Johnson potential (mBJ) is going to be utilized to improve the calculations of the total and partial density of state and energy band gaps. In addition to the previous studies, the elastic properties will be investigated for both compounds.

Previous studies on Co_2 MnSi and Co_2 MnGe Heusler compounds have focused only on the structural, magnetic, and electronic properties of the normal structure.

In this study, moreover to these properties, we investigate the elastic properties of both compounds. Furthermore, the structural, magnetic, electronic, and elastic properties of both compounds are examined at the inverse structure.

The mBJ method is essential for determining whether the compounds are semiconductors, insulators, metals, or half-metals. Understanding half-metallicity is particularly important for spin-polarized systems.

The elastic properties are critical for evaluating the stability of the compounds, bond nature, harmonic or anharmonic behavior, ductility, brittleness, and several other characteristics.

The methodology is detailed in chapter two. We will show our results and discussion in chapter three. Finally in chapter four conclusion is summarized.

Chapter Two

Methodology

In solids, to calculate the quantitative properties we need the solution of the time independent Schrödinger Equation (SE) for N-body system (36–38)

$$\hat{\mathrm{H}}\psi = \mathrm{E}\psi \tag{1}$$

where H is the Hamiltonian of N-body system, E is the energy for N-body system and Ψ is a wave function of all participating particles.

$$H = -\frac{\hbar^2}{2}\sum_{i=1}^{N}\frac{\nabla^2\vec{R}_i}{M_i} - \frac{\hbar^2}{2}\sum_{i=1}^{N}\frac{\nabla^2\vec{r}_i}{m_e} - \frac{1}{4\pi\epsilon_0}\sum_{ij}^{N}\frac{e^2 Z_i}{|\vec{R}_i - \vec{r}_i|} + \frac{1}{8\pi\epsilon_0}\sum_{i\neq j}^{N}\frac{e^2}{|\vec{r}_i - \vec{r}_j|} + \frac{1}{8\pi\epsilon_0}\sum_{i\neq j}^{N}\frac{e^2 Z_i Z_j}{|\vec{R}_i - \vec{R}_j|} \tag{2}$$

The first term in this equation is the nuclei's kinetic energy operator (T_n), the second one for the electrons (T_e). The last three terms described the coulomb interaction between electron and nuclei (V_{en}), electron and other electrons (V_{ee}), nuclei and other nuclei (V_{nn}) respectively.

This SE can't be solved exactly for N-body system. So here are some approximations to solve this problem:

2.1 The Born-Oppenheimer Approximation (BOA)

The Born-Oppenheimer Approximation assumed that the mass of nuclei is significantly larger than the mass of electron (39,40), therefore much slower than the electron, so that it is appears as fixed comparing with electron. So according to BOA T_n can be dropped and V_{nn} will be reduced to a constant.

Therefore equation (2) with applying BOA can be written as

$$\hat{\mathrm{H}} = \hat{T}_e + \hat{\mathrm{V}}_{\mathrm{en}} + \hat{\mathrm{V}}_{\mathrm{ee}} + \hat{\mathrm{V}}_{\mathrm{nn}} \tag{3}$$

$$\hat{\mathrm{H}} = \hat{T}_e + \hat{\mathrm{V}}_{\mathrm{ee}} + \hat{\mathrm{V}}_{\mathrm{ext}} \tag{4}$$

with fixed position of nuclei, where $V_{ext} = V_{en} + V_{nn}$ and called the external potential. The N-particle problem become simpler but it still difficult to calculate, and the complex represented in V_{ee} term.

2.2 Hartree and Hartree-Fock Approximation

Hartree approximation based on assuming that the electrons were independent of each other (40), so the wave function (ψ) of many electrons can be written as:

$$\psi_n(r_1, r_2, r_3, \dots, r_N) = \psi_1(r_1)\psi_2(r_2)\psi_3(r_3)\dots\psi_N(r_N) \quad (5)$$

where: $\Psi_N(r_N)$ is the wave function for the electrons.

depending on that total Hamiltonian can be expressed as:

$$\hat{H} = \hat{T}_e + \hat{V}_{ext} + \hat{V}_H \quad (6)$$

where T_e is the kinetic energy, V_{ext} is the external potential and V_H is the Hartree potential that can be written as:

$$\hat{V}_H = \frac{1}{8\pi\varepsilon_0}\sum_{ij}^{N}\frac{|\psi(\vec{r_i})|^2\left|\psi(\vec{r_j})\right|^2 d^3r_i d^3r_j}{\left|\vec{r_i} - \vec{r_j}\right|}. \quad (7)$$

The main problem with this method is that it needs a lot of computational prosses, that makes it a more complex system.

2.3 Density Functional Theory (DFT)

DFT have been established by Hohenberg and Kohn in 1964, it replaces the electron wave function of many electrons with the electron density as the basic quantity (41).

By DFT the N-body problem can be solved as a one-body problem (non-interacting system having the same total density). It's efficient reduction of the functional energy would lead to the density of the ground state (ρ_0).

Thus $E(\rho)$ can be redefined as the Hartree total energy plus another smaller unknown functional called exchanged-correlation functional $E_{xc}(\rho)$.

$$E(\rho) = T_s(\rho) + E_c(\rho) + E_H(\rho) + E_{ii}(\rho) + E_{xc}(\rho) \quad (8)$$

where T_s refers to single kinetic energy, E_c is coulomb energy between nuclei and electrons, $E_{ii}(\rho)$ the interaction between nuclei, E_{xc} is exchange correlation energy, which is an unknown part and E_H is Hartree potential.

$$E_H(\rho) = \frac{e^2}{2}\int d^3r\, d^3r' \, \frac{\rho(\vec{r})\rho(\vec{r'})}{|\vec{r} - \vec{r'}|} \quad (9)$$

SE for one electron can be written as:

$$\left[T_S + V_{ext}(r) + V_H\big(\rho(r)\big) + V_{XC}\big(\rho(r)\big)\right]\Phi_i(r) = \varepsilon_i\Phi_i(r) \quad (10)$$

where, ε_i is the single particle energy, Φ_i is the electron wave function, V_H is the Hartree potential, V_{ext} the coulomb potential and V_{XC} is the exchange-correlation potential.

2.4 Single particle Kohn-Sham Equation

Kohn-Sham (KS) equations of a N-electron system for the density of the ground state, total energy, and KS eigenvalues (energy bands) were solved by LAPW method (38).

This expression could be explained as the functional energy of a non-interacting classical electron gas, subjected into two external potentials: the first one is because of the nuclei $\hat{V}_{ext}[\rho]$, and the second is because of the exchange and correlation effects $\hat{V}_{xc}[\rho]$.

The exact ground-state density $\rho(r)$ of an N-electron system is:

$$\rho(\vec{r}) = \sum_{i=1}^{N}\phi_i^*(\vec{r})\phi_i(\vec{r}) = \sum_{i=1}^{N}|\phi_i(\vec{r})|^2, \quad (11)$$

where $\phi_i(\vec{r})$ is the single-particle wave functions, that are the N lowest-energy solutions of the KS equation

$$\hat{H}_{KS}\phi_i = \epsilon_i\phi_i \quad (12)$$

KS equation sometimes is written as:

$$\hat{\mathrm{H}}\phi_{\mathrm{i}}(\vec{\mathrm{r}}) = \left[-\frac{\hbar^2}{2\mathrm{m_e}}\vec{\nabla}_{\mathrm{i}}^2 + \mathrm{V_{eff}}\right]\phi_{\mathrm{i}} = \epsilon_{\mathrm{i}}\phi_{\mathrm{i}} \tag{13}$$

where $\hat{H}$ is the Hamiltonian operator. The effective potential $V_{eff}(\vec{\mathrm{r}})$ is the sum of the external, the Hartree (electrostatic), and the exchange-correlation potentials:

$$\begin{aligned}\mathrm{V_{eff}}(\vec{\mathrm{r}}) &= \mathrm{V_{ext}}(\vec{\mathrm{r}}) + \frac{\delta \mathrm{E_H}[\rho]}{\delta\rho} + \frac{\delta \mathrm{E_{xc}}[\rho]}{\delta\rho} \\ &= \mathrm{V_{ext}}(\vec{\mathrm{r}}) + \frac{\mathrm{e}^2}{4\pi\epsilon_0}\int \frac{\rho(\vec{\mathrm{r}'})}{|\vec{\mathrm{r}} - \vec{\mathrm{r}}'|}\mathrm{d}\vec{\mathrm{r}}' + \mathrm{V_{xc}}(\vec{\mathrm{r}})\end{aligned} \tag{14}$$

From the above equation, V_H and V_{xc} depends on the charge density $\rho(\vec{r})$, which depends on the ϕ_i that were being searched. That implies we were dealing with a self - consistency problem.

The solution ϕ_{i} obtain the original equation ($\mathrm{V_H}$ and V_{xc} in H_{ks}), It is impossible to write down an equation and solve it before knowing it's solution.

Some initial density ρ_0 is guessed, and a Hamiltonian $\mathrm{H_{KS1}}$ can be constructed through it. The eigenvalue problem is solved, and ϕ_1 can be determined from ρ_1. Now ρ_1 can be utilized to construct $\mathrm{H_{KS2}}$ that will lead to ρ_2, etc. The procedure can be used until the series converge and ρ_{f} get out (42). These steps are shown in figure (3).

Figure 3

Flow chart of the n^{th} repitition in the self-consistent procedure to solve Hartree-Fock or Kohn-Sham equations

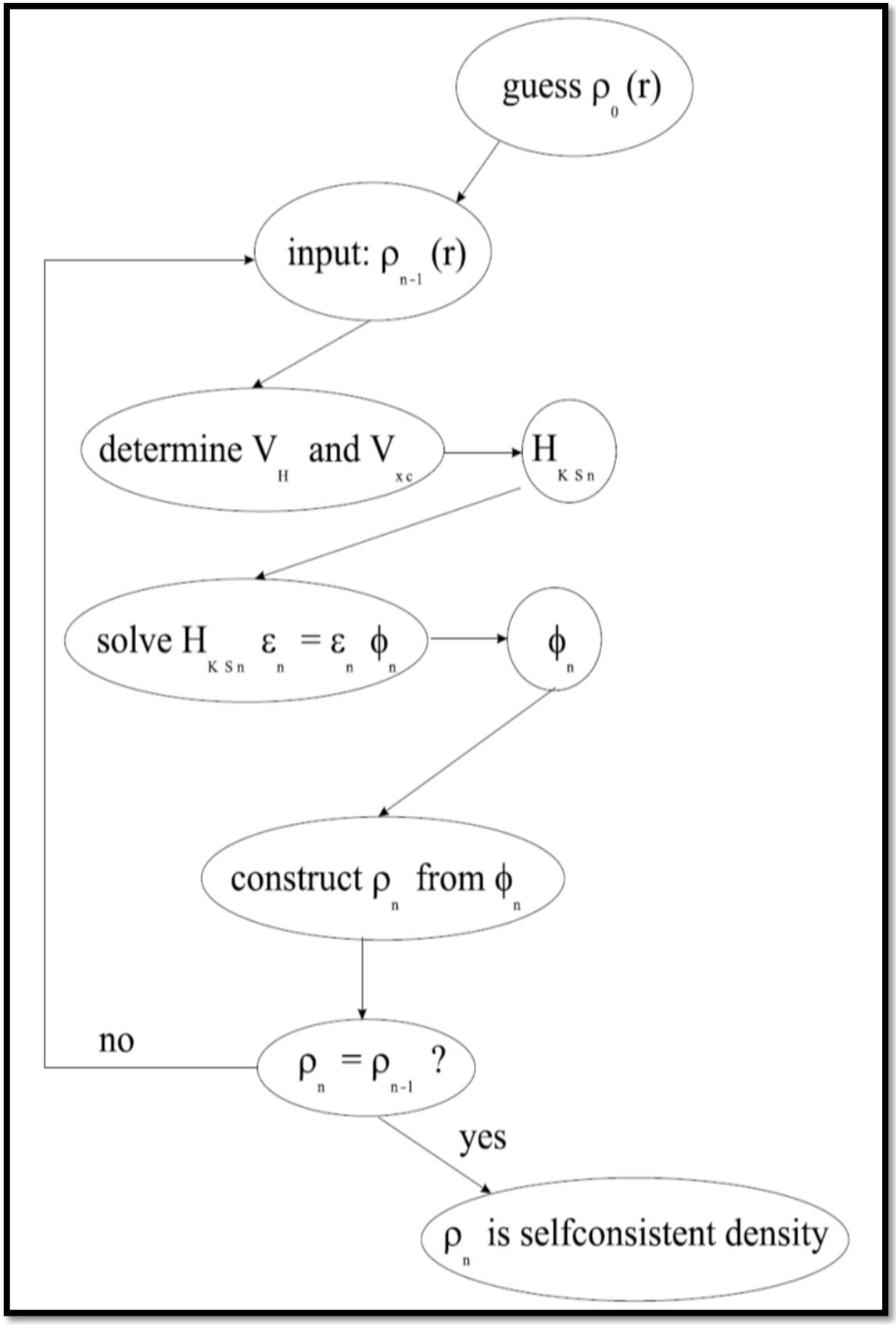

2.5 The Exchange-Correlation Functional

The Kohn-Sham scheme mentioned previously was accurate if no other approximations were made except the preceding Born-Oppenheimer approximation. But we don't know the functional exchange-correlation yet.

The introduction of an approximation is needed. Two such often-used approximations are Local Density Approximation (LDA) and Generalized Gradient Approximation (GGA) (38).

2.6 Local Density Approximation (LDA)

LDA was applied to DFT by Kohn and Sham. The functional exchange-correlation doesn't known exactly but can be estimated.

LDA can be solved by the exchange-correlation energy (43). The LDA for the exchange-correlation energy would be given as:

$$E_{xc}^{LDA} = \int \rho(\vec{r})\varepsilon_{xc}[\rho(\vec{r})]\, d\vec{r} \qquad (15)$$

where the $\varepsilon_{xc}[\rho(\vec{r})]$ is defined as the exchange-correlation energy per electron of a homogenous electron gas, whose electronic density is precisely $\rho_0(r)$ at any r.

The LDA approximation going to be valid when the electronic density changes very slowly with the position due to lack of ρ_0 (r) derivative in the expression for $\varepsilon_{xc}[\rho(\vec{r})]$, which indicates by the term "local".

If the exchange and correlation contributions are considered independently, the first contribution could be calculated analytically.

The Correlation energy, due to lacks analytic expression and it represented as a complex function of ρ_0 that depends on the parameters whose values were fitted using a precise simulation of the homogeneous electron gas energy as reference.

$$E_{xc}^{LDA} = E_{x}^{LDA} + E_{c}^{LDA} \qquad (16)$$

The first term is the exchange energy which comes from the Pauli Exclusion Principle, while the second term, called the correlation energy which comes from the interaction of electrons with the same spin (43).

2.7 Generalized Gradient Approximation (GGA)

GGA improves the local spin density (LSD) definition of the exchange-correlation energy through including the first derivatives of the electronic density (43).

While LDA uses the exchange energy density of the homogeneous electron gas, neglected of the homogeneity of the actual charge density, GGA takes care of such inhomogeneity by including the gradient of the electron density $\vec{\nabla}\rho(\vec{r})$ in the function.

$$E_{xc}^{GGA} = \int \rho(\vec{r})\varepsilon_{xc}\left[\rho(\vec{r}), \vec{\nabla}\rho(\vec{r})\right] d\vec{r} \qquad (17)$$

where $\rho(\vec{r})$ is the charge density, and $\nabla\rho(\vec{r})$ is the gradient of charge density. GGA was found to be more accurate than the LDA in electronic structure calculation.

2.8 Augmented Plane Wave (APW) Method

APW method is a procedure for solving the KS equation. In APW method (38), unit cell is splited into two types of areas. The first one is separated atomic spheres centered at the atomic sites such a sphere is called a muffin tin (S_α) with radius R_α. The second is the remaining space outside the spheres that are called the interstitial area.

These regions are displayed in figure (4).

Figure 4

Scheme of Augmented Plane Wave

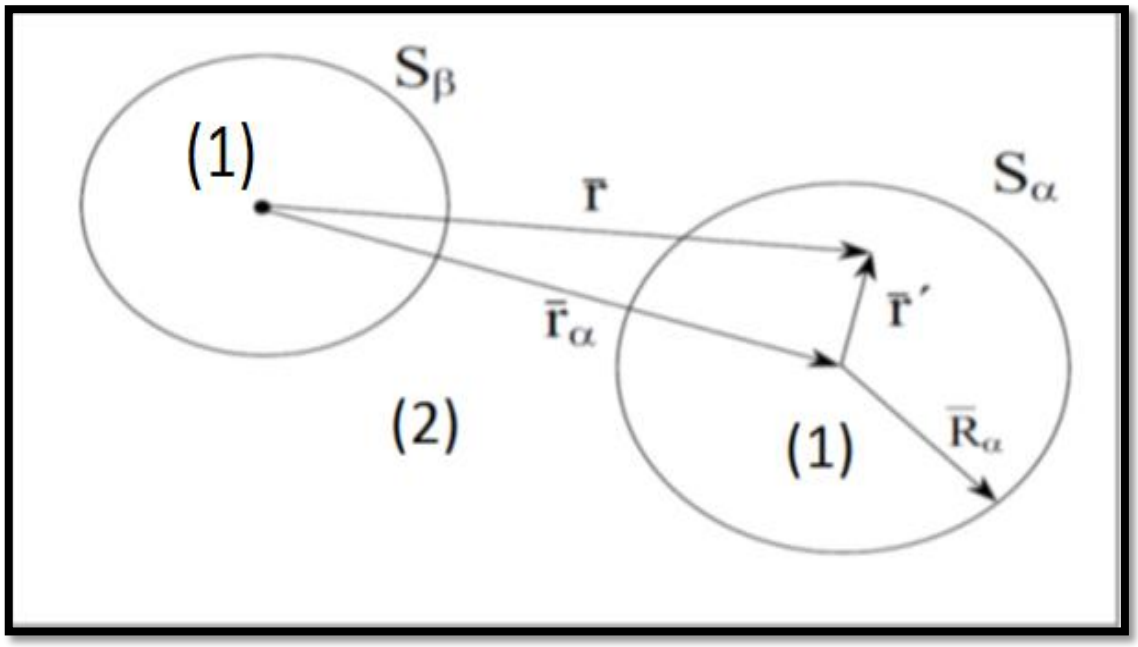

In the area far away from the nuclei, the electrons are approximately free so it can be described within plane waves. But if electrons are close to the nuclei, they behave quite as they were in a free atom, so they can be described within spherical harmonic functions.

APW used in the expansion of φ_n is defined as:

$$\boldsymbol{\phi}_{\vec{K}}^{\vec{k}}(\vec{r},\boldsymbol{E}) = \begin{cases} \dfrac{\mathbf{1}}{\sqrt{\boldsymbol{V}}}\boldsymbol{e}^{\boldsymbol{i}(\vec{k}+\vec{K}).\vec{r}}, \boldsymbol{r} > \mathrm{R}_\alpha \\ \sum_{\boldsymbol{l},\boldsymbol{m}} \boldsymbol{A}_{\boldsymbol{lm}}^{\boldsymbol{\alpha},\vec{k}+\vec{K}}\, \boldsymbol{u}_{\boldsymbol{l}}^{\boldsymbol{\alpha}}(\boldsymbol{r}',\boldsymbol{E})\boldsymbol{Y}_{\boldsymbol{l}}^{\boldsymbol{m}}(\hat{\boldsymbol{r}}'), \boldsymbol{r}' < \mathrm{R}_\alpha \end{cases} \tag{18}$$

Where $\vec{k}$ is the wave vector inside the Brillion zone, $\vec{K}$ is the reciprocal lattice vectors, V is the volume of the unit cell, r' is the position vector inside the sphere, and u_l^α is the radial part solution of SE at energy ε.

2.9 The Linearized Augmented Plane Wave (LAPW) Method

LAPW method is a procedure for solving the KS equation (38). Anderson was introduced to the LAPW scheme (look like APW scheme). He suggested expanding the energy dependence of radial wave functions u(r′) inside the atomic spheres with its energy derivative $\frac{\partial \mathrm{u}^\alpha(\mathrm{r}',\mathrm{E})}{\partial \mathrm{E}} = \dot{\mathrm{u}}^\alpha(\mathrm{r}',\mathrm{E})$, A linear combination of radial function times spherical harmonics is utilized in this scheme.

For a sphere of radius R_α, spherical harmonic $Y_{lm}(r)$ is used where $u_l(r,E_l)$ is the normal solution of the radial SE for energy $E_{l,}$ and the spherical part of the potential inside sphere $\dot{u}^\alpha(r',E)$ is the energy derivative of u_l taken at the same energy.

$$\phi_{\vec{K}}^{\vec{k}}(\vec{r},E) = \sum_{l,m}(a_{lm}^{\alpha,\vec{k}+\vec{K}}\, u_l^\alpha(r',E) + b_{lm}^{\alpha,\vec{k}+\vec{K}}\dot{u}_l^\alpha(r',E))\, Y_m^l(\hat{r}'), r' < R_\alpha \tag{19}$$

In the interstitial area this expansion for plane wave is used:

$$\boldsymbol{\phi}_{\vec{K}}^{\vec{k}}(\vec{r},\boldsymbol{E}) = \frac{\mathbf{1}}{\sqrt{\boldsymbol{V}}}\boldsymbol{e}^{\boldsymbol{i}(\vec{k}+\vec{K}).\vec{r}}, \boldsymbol{r} > \mathrm{R}_\alpha \tag{20}$$

In general form LAPW method expands the potential as the following formula:

$$V(\vec{r}) = \begin{cases} \sum_{lm} V_{lm}(r) Y_{lm}(\hat{r}) \text{ insidesphere} \\ \sum_{\vec{k}} V_{\vec{k}}\, e^{i\vec{k}.\vec{r}} \text{ outsidesphere} \end{cases} \quad (21)$$

2.10 Modified Becke-Johnson Potential (mBJ)

Because mBJ improves the band structure of materials, particularly semiconductor materials (44), it is a tool that is highly important and is applied in the WIEN2k code.

As a result, it is significant in terms of general agreement with the experiment. Due to the absence of an exchange and correlation energy term from which to deduce the mBJ-GGA potential, a straight optimization to determine the lattice parameter is not feasible.

The experimental gap value can deviate by as much as 20-40 percent. It was proposed that the LDA, GGA optimization approach was previously utilized to compute the band structure and the resulting lattice parameter, and this suggestion is important because small percentage differences in the lattice parameter can result in higher relative deviations from experimental in the expected band gap.

Chapter Three

Results and Discussion

3.1 Computational Method

The full potential linearized augmented plane wave method (FP-LAPW) which implemented in Wien2k package(38), within generalized gradient approximation (PBE-GGA) has been used in this work.

For Co_2MnSi compound Co, Mn and Si atoms have muffin-tin radii (R_{MT}) 2.18,2.18 and 2.01 a.u., consequently, while in Co_2MnGe compound Co, Mn and Ge atoms have R_{MT} of 2.22,2.22 and 2.16 a.u., consequently.

To achieve a self-consistency for Co_2MnSi and Co_2MnGe 165 special k-points in the irreducible Brillion zone (IBZ) have been used with a grid equivalent to 5000 k-points in the overall BZ.

Moreover, the number of plane waves has been limited by $K_{max} * R_{MT} = 8$, while the wave functions expansions have been set to l = 10 inside the muffin tin spheres.

The self-consistent computations have been determined to have converge only when the computated total energy of the crystal converged to lower than 10^{-2} mRy.

Lastly, the elastic constants C_{11}, C_{12} and C_{44} have been computed by using the second-order derivative within the IRelast (45) formalism at Wien2k code.

$$C_{ij} = \frac{1}{V_0}\left[\frac{\partial^2 E}{\partial\varepsilon_i \partial\varepsilon_j}\right]_{\varepsilon_k=0} \quad (22)$$

Where Eis the energy of strained system and can be written as

$$E(V, \varepsilon_k) = E_0 + V_0\left[\sum_{i=1}^{6}\sigma_i\,\varepsilon_i + \frac{1}{2}\sum_{ij=1}^{6} C_{ij}\varepsilon_i\varepsilon_j\right] \quad (23)$$

Where ε_k is the energy and V is the volume of strained system.

3.2 Structural Properties

Computation of the structural properties; optimized lattice constant (a), bulk modulus (B), its pressure derivative (B′), and minimal energy $\boldsymbol{E_0}$. The total energy (Ry) versus volume (a.u^3) graphs have been fitted by utilizing Murnaghan's equation of state (EOS) which presented by (32):

$$E(V) = E_0 + \frac{VB}{\mathrm{B}'}\left\{\left[\frac{\left(\frac{V_0}{V}\right)^{\mathrm{B}'}}{\mathrm{B}'-1}\right] + 1\right\} - \left[\frac{BV_0}{\mathrm{B}'-1}\right] \qquad (24)$$

Where Pressure, P = - $\frac{dE}{dV}$, Bulk modulus, B = - V $\frac{dP}{dV}$ = V $\frac{d^2E}{dV^2}$

Normal Heusler Co_2MnSi and Co_2MnGe compounds with the space group Fm-3m L_{21} (225), where inverse Heusler Co_2MnSi and Co_2MnGe compounds have space group F-43m X (216) (46). Figure (5) indicates the full Heusler Co_2MnSi and Co_2MnGe compounds crystal structures.

During the optimization volume calculation, estimates of the lattice parameter have been determined for both normal and inverse Co_2MnSi and Co_2MnGe compounds.

The total energy versus the volume of Co_2MnSi and Co_2MnGe compounds in both normal and inverse structures are appeared in figure (6(a-d)).

The calculated structural properties for normal and invers Co_2MnSi and Co_2MnGe Heusler compounds are tabulated in table (1).

Figure 5

Crystal structures of the full Heusler Co_2MnSi and Co_2MnGe compounds (red: Co, blue: Mn, green: Si / Ge)

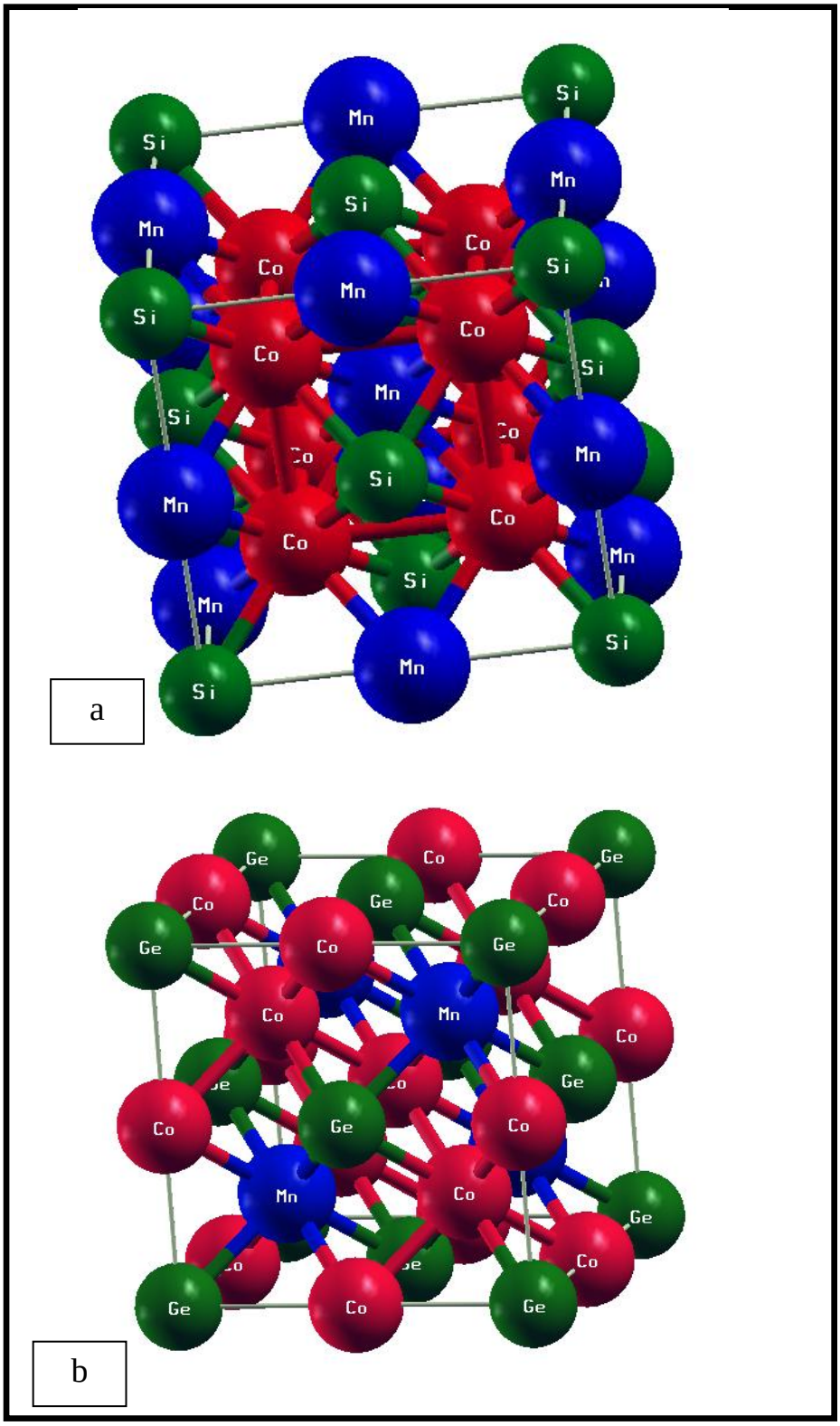

Note: (a) normal Heusler (L_{21}) and (b) inverse Heusler (Xa),

Figure 6

The total energy (Ry) versus volume (a.u^3) of Heusler compounds

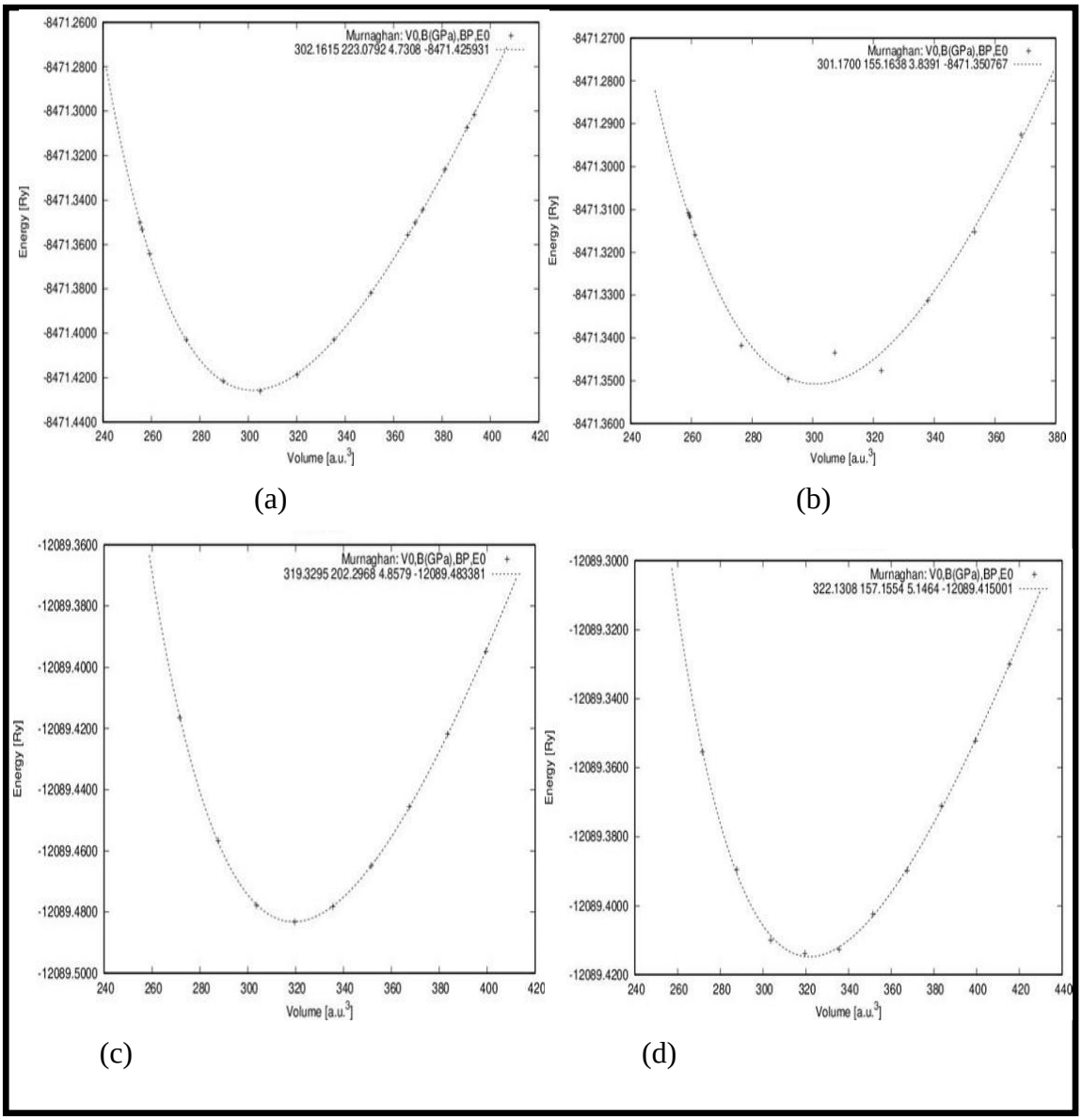

Note: (a) normal Co_2MnSi, (b) inverse Co_2MnSi, (c) normal Co_2MnGe and (d) inverse Co_2MnGe.

Table 1

Calculated lattice parameter(a), bulk modulus (B), first pressure derivative of the Bulk modulus (B') and minimum energy E_0 for normal and inverse Heusler Co_2MnSi and Co_2MnGe Heusler compounds

Compounds	Space group	Reference	a (Å)	B (GPa)	B'(GPa)	E_0 (eV)
Co_2MnSi	Normal Fm-3m (225)	Present	5.6347	226.5334	5.2684	-8471.426864
		Experimental	5.654 (32,34)			
			5.661 (33)			
			5.620 (32)			
		Theoretical	5.694 (34)			
			5.63 (35)			
	Inverse F-43m (216)	Present	5.6459	180.7051	-0.6028	-8471.355770
Co_2MnGe	Normal Fm-3m (225)	Present	5.7351	200.9877	5.5049	-12089.414823
		Experimental	5.743 (32,34)			
		Theoretical	5.727 (32)			
			5.825 (34)			
	Inverse F-43m (216)	Present	5.7528	125.9760	20.6020	-12089.389507

Table (1) show that the lattice parameter is 5.6347, 5.7351, 5.6459 and 5.7528 A^0 for normal Co_2MnSi, normal Co_2MnGe, inverse Co_2MnSi and inverse Co_2MnGe respectively.

Table (1) indicate a good agreement between present results and experimental lattice parameter for both normal compounds. For normal Co_2MnSi compound our result is 0.34% smaller than experimental lattice parameter, but for normal Co_2MnGe compound it is 0.14% smaller than experimental.

According to minimum energy (E_0), table (1) shows that E_0 is -8471.426864, -12089.414823, -8471.355770 and -12089.389507 eV for normal Co_2MnSi, normal Co_2MnGe, inverse Co_2MnSi and inverse Co_2MnGe respectively.

From table (1) we can notice that normal Co_2MnSi compound has minimal energy E_0 less than inverse structure, which mean comparing to the inverse structure, the normal structure is more mechanically stable.

The same for Co_2MnGe compound, E_0 for normal structure lower than inverse structure, which mean comparing to the inverse structure, the normal structure is more mechanically stable.

The bulk modulus for normal Co_2MnSi, normal Co_2MnGe, inverse Co_2MnSi and inverse Co_2MnGe is 226.5334, 200.9877, 180.7051 and 125.9760 GPa respectively. And its first derivative is 5.2684, 5.5049, -0.6028 and 20.6020 GPa for normal Co_2MnSi, normal Co_2MnGe, inverse Co_2MnSi and inverse Co_2MnGe respectively.

The previous studies found the lattice parameter only, this study has a good agreement with the earlier results.

In addition to that, this study found the bulk modulus, it's first derivative and the minimum energy for both normal and inverse Co_2MnSi and Co_2MnGe full Heusler compounds. Moreover the lattice parameter for inverse Co_2MnSi and inverse Co_2MnGe full Heusler compounds were founded in this study.

3.3 Magnetic Properties

The total and partial magnetic moment of normal and inverse Heusler compounds Co_2MnSi and Co_2MnGe have been calculated using GGA, and the result have been compared with other previous studies, as mentioned in table (2). In addition, mBJ used to prove that compounds are half metallic or not, and the result mentioned in table (3).

The total magnetic moment of normal Co_2MnSi, normal Co_2MnGe, inverse Co_2MnSi and inverse Co_2MnGe is 4.99382, 4.96698, 4.31954 and 4.97734 μ_B respectively.

In contrast, the partial magnetic moment firstly of normal Co_2MnSi compound is 1.06500, 2.95095, -0.04115 and -0.04597 μ_B for both Co atom, Mn atom, Si atom and interstitial respectively.

Then for normal Co_2MnGe compound it's 1.01069, 3.01243, -0.03382 and -0.03301 μ_B for both Co atom, Mn atom, Ge atom and interstitial respectively.

Moreover, partial magnetic moment is 0.89886, 1.68790, 1.84580, -0.03163 and -0.08139 μ_B for first Co atom, second Co atom, Mn atom, Si atom and interstitial respectively at inverse Co_2MnSi compound.

Finally, at inverse Co_2MnGe compound it's 1.03149, 1.64726, 2.39885, -0.03439 and -0.06587 μ_B for first Co atom, second Co atom, Mn atom, Ge atom and interstitial respectively.

From table (2) we notice that both normal and inverse Heusler compounds Co_2MnSi and Co_2MnGe are ferromagnetic materials.

In Co_2MnSi, the total magnetic moment in normal structure is larger than that in inverse structure because of the high contribution of Mn atom in the normal case.

Table (2) indicates that the main contribution in the total magnetic moment of both normal and inverse Heusler Co_2MnGe compound is from Mn atom.

Table (2) shows a good agreement between present results and previous experimental total magnetic moment for both compounds Co_2MnSi and Co_2MnGe. For Co_2MnSi our result is 1.503 % lower than the experimental result, and for Co_2MnGe it is 2.799 % lower than experimental one.

Table 2

Total, atomic and interstitial GGA magnetic moment of normal and inverse Heusler compounds Co_2MnZ where Z (Si. Ge)

Structure	Reference	Magnetic Moment in (μ_B)					
		Co_1	Co_2	Mn	Z	Interstitial	Total magnetic moment (M^{tot})
Normal Co_2MnSi	Present	1.06500	1.06500	2.95095	-0.04115	-0.04597	4.99382
	Experimental						5.07 (34)
	Theoretical	1.07 (32,35) 1.021 (8) 0.893 (34)	1.07 (32,35) 1.021 (8) 0.893 (34)	2.95 (32) 2.971 (8) 3.253 (34) 2.85 (35)	-0.074 (8) -0.037 (34) -0.04 (35)		4.940 (8) 5 (34,35)
Inverse Co_2MnSi	Present	0.89886	1.68790	1.84580	-0.03163	-0.08139	4.31954
Normal Co_2MnGe	Present	1.01069	1.01069	3.01243	-0.03382	-0.03301	4.96698
	Experimental						5.11 (34)
	Theoretical	1.03 (32) 0.981 (8) 0.901 (34)	1.03 (32) 0.981 (8) 0.901 (34)	3.02 (32) 3.04 (8) 3.393 (34)	-0.061 (8) -0.196 (34)		4.941 (8) 5 (34)
Inverse Co_2MnGe	Present	1.03149	1.64726	2.39885	-0.03439	-0.06587	4.97734

Table 3

Total, atomic and interstitial mBJ magnetic moment for normal and inverse Heusler compounds Co_2MnZ where Z (Si. Ge)

Structure	Reference	Magnetic Moment in (μ_B)					
		Co_1	Co_2	Mn	Z	Interstitial	Total magnetic moment (M^{tot})
Normal Co_2MnSi	Present	1.17379	1.17379	3.02703	-0.07775	-0.29688	4.99999
Inverse Co_2MnSi	Present	1.08738	2.02467	1.95504	-0.06462	-0.21975	4.78272
Normal Co_2MnGe	Present	1.15090	1.15090	3.10702	-0.07531	-0.33358	4.99994
Inverse Co_2MnGe	Present	1.34288	1.98689	3.05165	-0.05403	-0.18791	6.13948

Table (3) indicates the total, atomic and interstitial magnetic moment of both normal and inverse Heusler compounds Co_2MnSi and Co_2MnGe with mBJ approximation.

Total magnetic moment is 4.99999, 4.78272, 4.99994 and 6.13948 μ_B for normal Heusler compound Co_2MnSi, invers Heusler compound Co_2MnSi, normal Heusler compound Co_2MnGe and invers Heusler compound Co_2MnGe respectively.

In contrast, the partial magnetic moment firstly of normal Co_2MnSi compound is 1.17379, 3.02703, -0.07775 and -0.29688 μ_B for both Co atom, Mn atom, Si atom and interstitial respectively.

Then for normal Co_2MnGe compound it's 1.15090, 3.10702, -0.07531 and -0.33358 μ_B for both Co atom, Mn atom, Ge atom and interstitial respectively.

Moreover, partial magnetic moment is 1.08738, 2.02467, 1.95504, -0.06462 and -0.21975 μ_B for first Co atom, second Co atom, Mn atom, Si atom and interstitial respectively at inverse Co_2MnSi compound.

Finally, at inverse Co_2MnGe compound it's 1.34288, 1.98689, 3.05165, -0.05403 and -0.18794 μ_B for first Co atom, second Co atom, Mn atom, Ge atom and interstitial respectively.

From table (3) we notice that both normal and inverse Heusler compounds Co_2MnSi and Co_2MnGe are ferromagnetic materials.

In Co_2MnSi, the total magnetic moment in normal structure is larger than that in inverse structure because of the high contribution of Mn atom in the normal case.

Table (3) indicates that the main contribution in the total magnetic moment of normal and inverse Heusler Co_2MnGe compound is from Mn atom.

By comparing table (2) and table (3), we notice the impact of mBJ approximation on the magnetic moment of both normal and inverse Heusler compounds Co_2MnSi and Co_2MnGe. Moreover, total magnetic moment for both normal Heusler compounds Co_2MnSi and Co_2MnGe nearly integer, that means the compounds are half metallic.

The total magnetic moment for normal Co_2MnSi is 0.124 % larger by mBJ approximation than GGA. For normal Co_2MnGe it's 0.664 % larger by mBJ

approximation than GGA. Moreover, for inverse Co_2MnSi the total magnetic moment is 10.723 % larger by mBJ approximation than GGA. Also, it's 23.349 % larger by mBJ approximation than GGA for inverse Co_2MnGe.

The previous studies found the total and partial magnetic moment of normal Heusler compounds Co_2MnSi and Co_2MnGe by GGA only. In addition to that, in this study the total and partial magnetic moment of inverse Heusler compounds Co_2MnSi and Co_2MnGe by GGA. Moreover, the total and partial magnetic moment of normal and inverse Heusler compounds Co_2MnSi and Co_2MnGe by mBJ approximating.

3.4 Electronic Properties

In this section, the band structure (BS), the partial density of states (PDOS) and the total density of states (TDOS) were investigated for both normal and inverse Heusler Co_2MnSi and Co_2MnGe Heusler compounds using GGA. Also using mBJ to enhance band gsp.

The analysis of the BS for normal Heusler structures of Co_2MnSi and Co_2MnGe investigated that they behave half-metallically. It is metallic in spin-up with zero band gap, and semiconductor in spin-down, using both GGA-PBE and mBJ-GGA techniques.

The BS for inverse Heusler structures of Co_2MnSi and Co_2MnGe indicated that they behave metallically with zero band gap in both spin-up and spin down, using GGA-PBE and mBJ-GGA techniques.

Figures (**7**-**10**) showed the band structure for both normal and inverse Co_2MnSi and Co_2MnGe Heusler compounds.

Table 4

Band gap of normal and inverse Heusler compounds Co_2MnSi and Co_2MnGe

Compound	Reference	E_g GGA (eV)	E_g mBJ (eV)	E_g Type
Normal Co_2MnSi	Present	0.819	1.471	direct
	Theoretical	0.69 (34) 0.83 (35)		
Inverse Co_2MnSi	Present	0	0	
Normal Co_2MnGe	Present	0.578	1.551	direct
	Theoretical	0.58 (34)		
Inverse Co_2MnGe	Present	0	0	

Table (4) shows the energy band gap for both normal and invers Heusler compounds Co_2MnSi and Co_2MnGe by both approximations GGA and mBJ.

The energy band gap for normal Co_2MnSi and normal Co_2MnGe is 0.819 and 0.875 eV respectively by GGA for spin down, these two compounds are metallic for spin up with zero energy band gap. According these band gaps both normal Heusler compounds Co_2MnSi and Co_2MnGe are half metallic compounds.

Both inverse Heusler compounds Co_2MnSi and Co_2MnGe have zero energy band gap, so both of these compounds are metallic compounds.

Table (4) indicates a good agreement between previous studies and our study. For normal Co_2MnSi present energy band gap is 18.696 % and 1.325 % lower than previous studies. For normal Co_2MnGe it's 0.345 % lower than previous study.

Previous studies found the energy band gap for both normal Co_2MnSi and Co_2MnGe by GGA only.

In addition to that, this study found the energy band gap of both inverse Heusler compounds by GGA. Moreover, the energy band gap of both normal and inverse Heusler Compounds Co_2MnSi and Co_2MnGe by mBJ approximation.

Table (4) indicates the effect of mBJ approximation on the computed energy band gap of both normal Heusler Co_2MnSi and Co_2MnGe.

Energy band gap for normal Co_2MnSi is 79.609 % larger by mBJ approximation than by GGA. And for normal Co_2MnGe it's 168.339 % larger by mBJ approximation than by GGA.

Figure 7

Band structure of normal Co_2MnSi

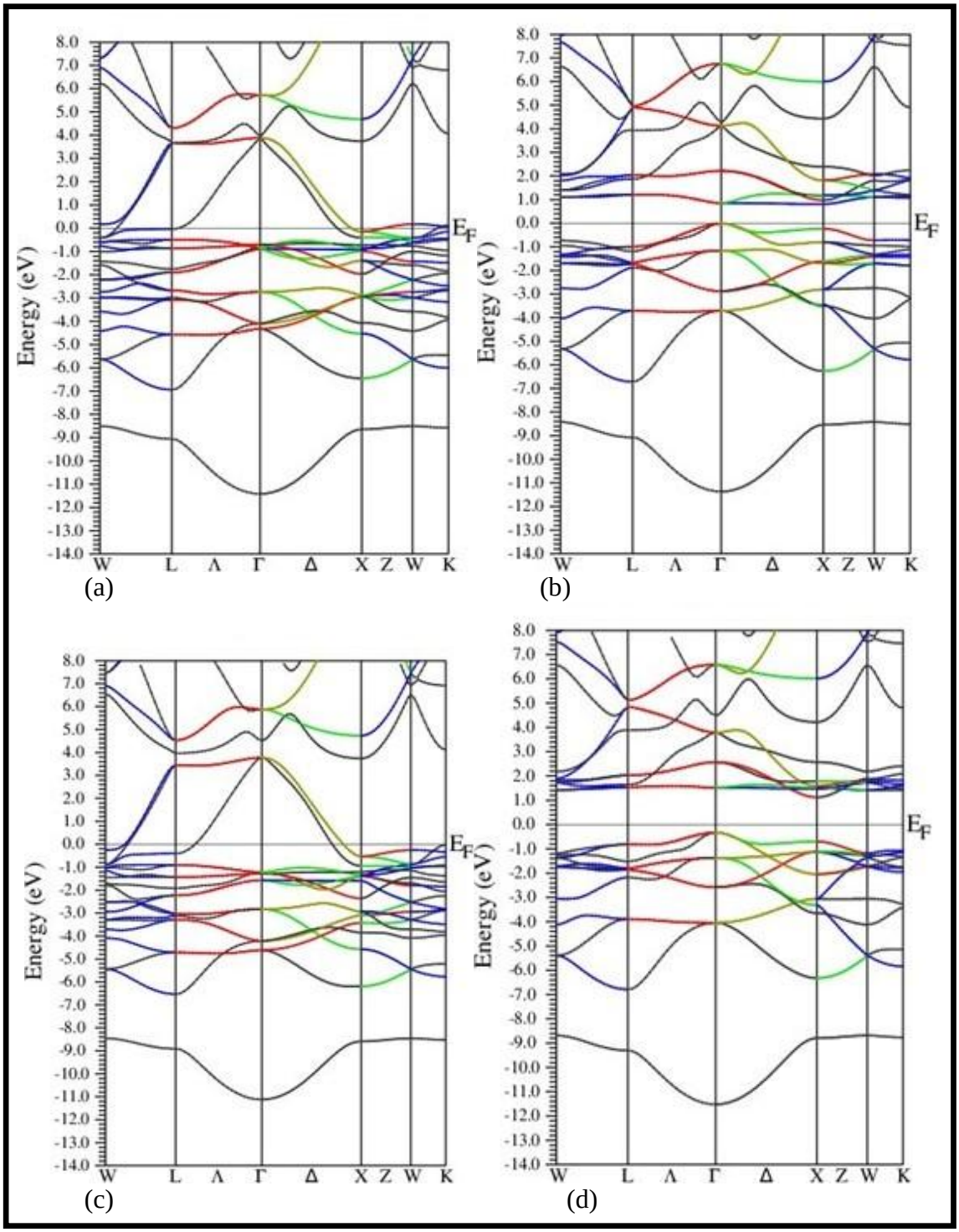

Note: (a) spin-up with GGA, (b) spin-down with GGA, (c) spin-up with mBJ and (d) spin-down with mBJ.

Figure 8

Band structure of inverse Co_2MnSi

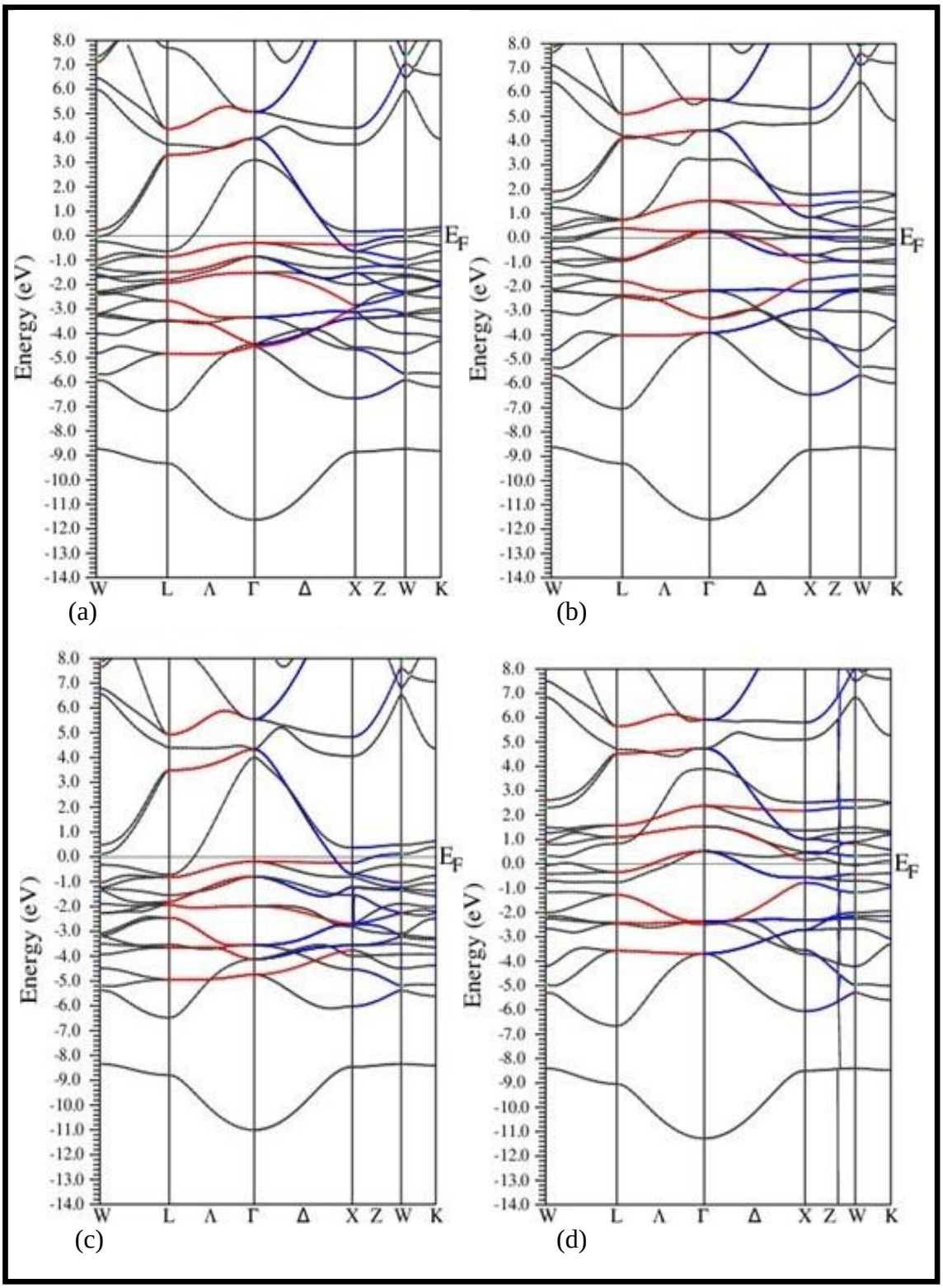

Note: (a) spin-up with GGA, (b) spin-down with GGA, (c) spin-up with mBJ and (d) spin-down with mBJ.

Figure 9

Band structure of normal Co_2MnGe

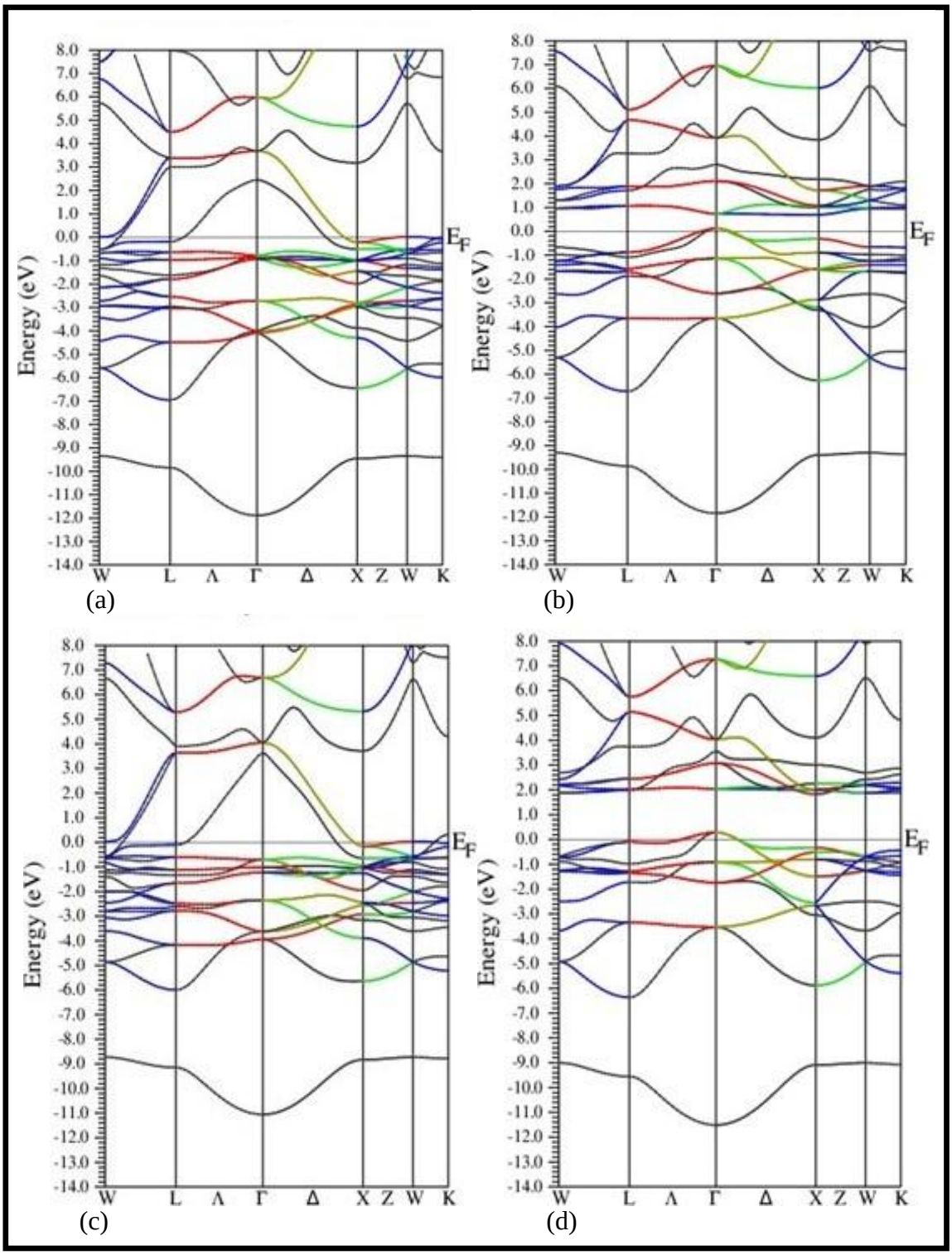

Note: (a) spin-up with GGA, (b) spin-down with GGA, (c) spin-up with mBJ and (d) spin-down with mBJ.

Figure 10

Band structure of inverse Co_2MnGe

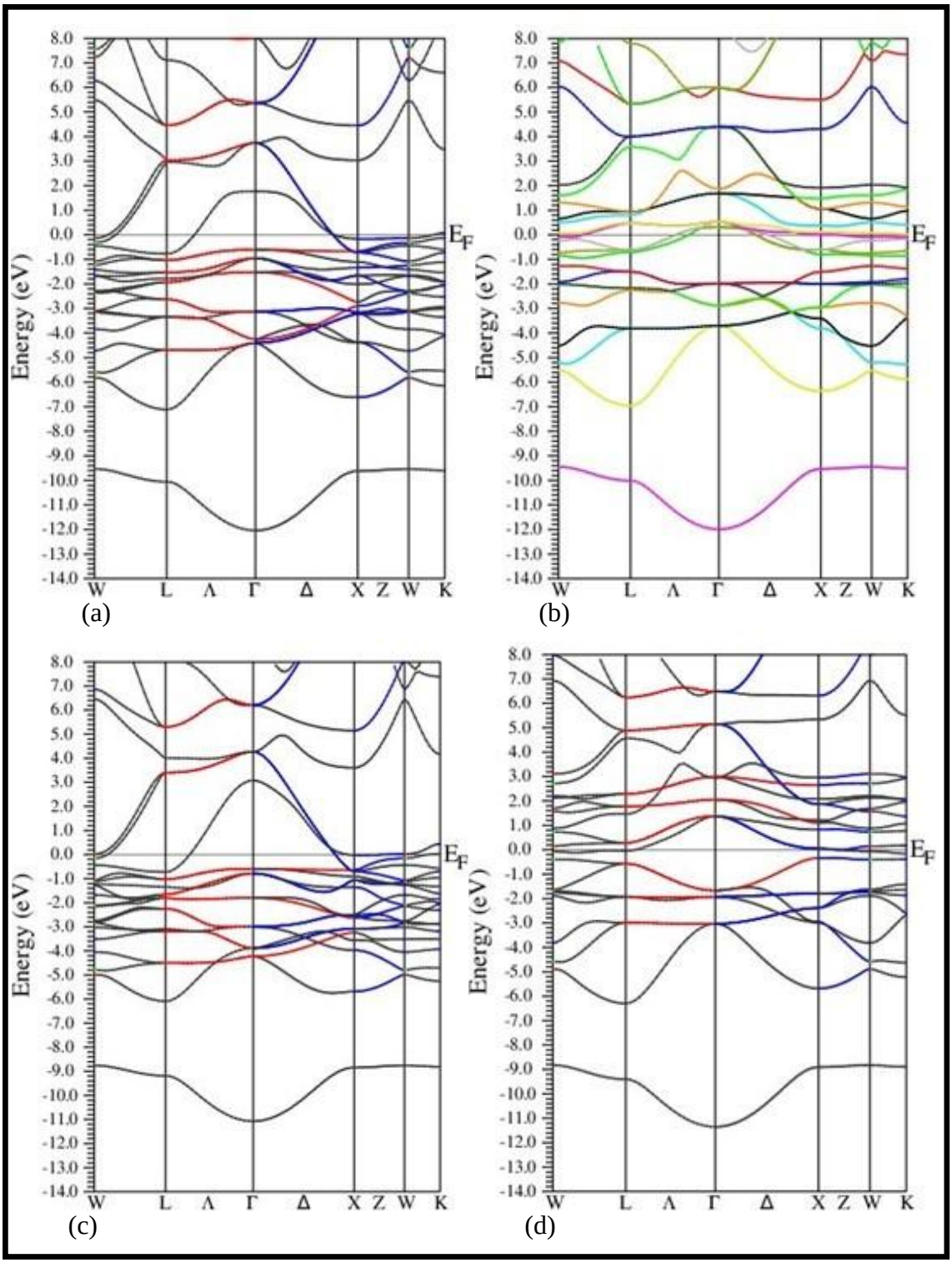

Note: (a) spin-up with GGA, (b) spin-down with GGA, (c) spin-up with mBJ and (d) spin-down with mBJ.

Figure 7 (a) indicated that the normal Heusler compound Co_2MnSi is metallic in spin up with no band gap, figure 7 (b) showed that this compound is semiconductor in spin down, which means the compound is half metallic.

Comparing figures 7 (b) and 7 (d) indicated the effect of mBJ method according to the band gap, it's clear that mBJ method improved the band structure of normal Co_2MnSi compound at spin-down.

Figure 8 showed that inverse Heusler compound Co_2MnSi is metallic with no band gap at both spin-up and spin-down, and the effect of mBJ method not clear because the compound is metallic.

Figure 9 (a) indicated that the normal Heusler compound Co_2MnGe is metallic in spin up with no band gap, figure 9 (b) showed that this compound is semiconductor in spin down, which means the compound is half metallic.

Comparing figures 9 (b) and 9 (d) indicated the effect of mBJ method according to the band gap, it's clear that mBJ method improved the band structure of normal Co_2MnSi compound at spin-down.

Figure 10 showed that inverse Heusler compound Co_2MnSi is metallic with no band gap at both spin-up and spin-down, and the effect of mBJ method not clear because the compound is metallic

For both normal Co_2MnSi and Co_2MnGe compounds at spin-up, the effect of mBJ doesn't appear clearly, because these compounds are metallic at spin-up and have zero energy gap.

Total and partial density of states for both normal and inverse Co_2MnSi and Co_2MnGe Heusler compounds in both spin-up and spin-down using GGA were appeared in figures (11 – 18) in appendix A.

Figure (11) in appendix A showed TDOS and PDOS of normal Co_2MnSi at spin-up. For spin-up the main contributions to the valence band (VB) is because of d-state of Co, d-state of Mn and p-state of Si. The major contributions of VB are from Co atom, then Mn atom and then a little contribution from Si atom for normal Co_2MnSi compound.

Moreover, the major contributions to the conduction band (CB) is because of d-state of Co, d-state of Mn and p-state of Si. The major contributions of CB are from Co atom, then Mn atom and then a little contribution from Si atom for normal Co_2MnSi compound.

Figure (12) in appendix A showed TDOS and PDOS of normal Co_2MnSi at spin-down. For spin-down the major contributions of the VB is because of d-state of Co, d-state of Mn and p-state of Si. The major contributions of VB are from Co atom, then Mn atom and then a little contribution from Si atom for normal Co_2MnSi compound.

Furthermore, the major contribution to the CB is because of d-state of Co, d-state of Mn and both s and p-state of Si. The major contributions of CB are from Co atom, then Mn atom and then a little contribution from Si atom for normal Co_2MnSi compound.

Figures (11) and (12) in appendix A showed that normal Co_2MnSi Heusler compound has a half-metallic behavior, it's metallic at spin-up with no band gap, and semi-conductor at spin-down with small band gap.

Figure (13) in appendix A showed TDOS and PDOS of inverse Co_2MnSi at spin-up. For spin-up the major contributions of the VB is because of d-state of Co, d-state of Mn and p-state of Si. The major contributions of VB are from Co atom, then Mn atom and then a little contribution from Si atom for inverse Co_2MnSi compound.

Moreover, the major contributions of the CB are because of d-state of Mn, d-state of Co and both s and p-state of Si. The major contributions of CB are from Mn atom, then Co atom and then a little contribution from Si atom for inverse Co_2MnSi compound.

Figure (14) in appendix A showed TDOS and PDOS of invers Co_2MnSi at spin-down. For spin-down the major contributions of the VB is because of d-state of Co, d-state of Mn and p-state of Si. The major contributions of VB are from Co atom, then Mn atom and then a little contribution from Si atom for invers Co_2MnSi compound.

Also, the major contributions of the CB are because of d-state of Mn, d-state of Co and both s and p-state of Si. The major contributions of CB are from Mn atom, then Co atom, then a little contribution from Si atom for invers Co_2MnSi compound. But near

fermi level the major contribution comes from Co atom. But near fermi level the major contribution comes from Co atom.

Figure (15) in appendix A showed TDOS and PDOS of normal Co_2MnGe at spin-up. For spin-up the major contributions of the VB is because of d-state of Co, d-state of Mn and p-state of Ge. The major contributions of VB are from Co atom, then Mn atom and then a little contribution from Ge atom for normal Co_2MnGe compound.

Also, the major contribution of the CB is because of d-state of Co, d-state of Mn and both s and p-state of Ge. The major contributions of CB are from Co atom, then Mn atom and then a little contribution from Ge atom for normal Co_2MnGe compound.

Figure (16) in appendix A showed TDOS and PDOS of normal Co_2MnGe at spin-down. For spin-down the major contributions of the VB is because of d-state of Co, d-state of Mn and p-state of Ge. The major contributions of VB are from Co atom, then Mn atom and then a little contribution from Ge atom for normal Co_2MnGe compound.

Moreover, the major contribution of the CB is because of d-state of Co, d-state of Mn and both s and p-state of Ge. The major contributions of CB are from Co atom, then Mn atom and then a little contribution from Ge atom for normal Co_2MnGe compound.

Figures (15) and (16) in appendix A showed that normal Co_2MnGe Heusler compound has a half-metallic behavior, it's metallic at spin-up with zero band gap, and semi-conductor at spin-down with small band gap.

Figure (17) in appendix A showed TDOS and PDOS of inverse Co_2MnGe at spin-up. For spin-up the major contributions of the VB is because of d-state of Co, d-state of Mn and p-state of Ge. The major contributions of VB are from Co atom, then Mn atom and then a little contribution from Ge atom for inverse Co_2MnGe compound. But near fermi level the major contribution comes from Mn atom.

Furthermore, the major contribution of the CB is because of d-state of Mn, d-state of Co and both s and p-state of Ge. The major contributions of CB are from Mn atom, then Co atom and then a little contribution from Ge atom for inverse Co_2MnGe compound.

Figure (18) in appendix A showed TDOS and PDOS of invers Co_2MnGe at spin-down. For spin-down the major contributions of the VB is because of d-state of Co, d-state of

Mn and p-state of Ge. The major contributions of VB are from Co atom, then Mn atom and then a little contribution from Ge atom for inverse Co_2MnGe compound.

On the other hand, the major contributions of the CB is because of d-state of Mn, d-state of Co and both s and p-state of Ge. The major contributions of CB are from Mn atom, then Co atom and then a little contribution from Ge atom for inverse Co_2MnGe compound. But near fermi level the major contribution comes from Co atom.

Figures (13), (14), (17) and (18) in appendix A indicated the metallic behavior for both inverse Co2MnSi and Co_2MnGe Heusler compounds, both of inverse compounds have zero band gap in both spin-up and spin-down.

Total and partial density of states for both normal and inverse Co_2MnSi and Co_2MnGe Heusler compounds in both spin-up and spin-down using mBJ were appeared in figures (19 – 26) in appendix A.

Figure (19) in appendix A showed TDOS and PDOS of normal Co_2MnSi at spin-up. For spin-up the main contributions to the valence band (VB) is because of d-state of Co, d-state of Mn and p-state of Si. The major contributions of VB are from Co atom, then Mn atom and then a little contribution from Si atom for normal Co_2MnSi compound.

Moreover, the major contributions to the conduction band (CB) is because of d-state of Co, d-state of Mn and p-state of Si. The major contributions of CB are from Co atom, then Mn atom and then a little contribution from Si atom for normal Co_2MnSi compound.

Figure (20) in appendix A showed TDOS and PDOS of normal Co_2MnSi at spin-down. For spin-down the major contributions of the VB is because of d-state of Co, d-state of Mn and p-state of Si. The major contributions of VB are from Co atom, then Mn atom and then a little contribution from Si atom for normal Co_2MnSi compound.

Furthermore, the major contribution to the CB is because of d-state of Co, d-state of Mn and p-state of Si. The major contributions of CB are from Co atom, then Mn atom and then a little contribution from Si atom for normal Co_2MnSi compound.

Figures (19) and (20) in appendix A showed that normal Co_2MnSi Heusler compound has a half-metallic behavior, it's metallic at spin-up with no band gap, and semi-conductor at spin-down with small band gap.

Figure (21) in appendix A showed TDOS and PDOS of inverse Co_2MnSi at spin-up. For spin-up the major contributions of the VB is because of d-state of Co, d-state of Mn and p-state of Si. The major contributions of VB are from Co atom, then Mn atom and then a little contribution from Si atom for inverse Co_2MnSi compound. But near fermi level the major contribution comes from Mn atom.

Moreover, the major contributions of the CB are because of d-state of Mn, d-state of Co and both s and p-state of Si. The major contributions of CB are from Mn atom, then Co atom and then a little contribution from Si atom for inverse Co_2MnSi compound.

Figure (22) in appendix A showed TDOS and PDOS of invers Co_2MnSi at spin-down. For spin-down the major contributions of the VB is because of d-state of Co, d-state of Mn and p-state of Si. The major contributions of VB are from Co atom, then Mn atom and then a little contribution from Si atom for invers Co_2MnSi compound.

Also, the major contributions of the CB are because of d-state of Mn, d-state of Co and both s and p-state of Si. The major contributions of CB are from Mn atom, then Co atom, then a little contribution from Si atom for invers Co_2MnSi compound. But near fermi level the major contribution comes from Co atom.

Figure (23) in appendix A showed TDOS and PDOS of normal Co_2MnGe at spin-up. For spin-up the major contributions of the VB is because of d-state of Co, d-state of Mn and p-state of Ge. The major contributions of VB are from Co atom, then Mn atom and then a little contribution from Ge atom for normal Co_2MnGe compound.

Also, the major contribution of the CB is because of d-state of Co, d-state of Mn and both s and p-state of Ge. The major contributions of CB are from Co atom, then Mn atom and then a little contribution from Ge atom for normal Co_2MnGe compound.

Figure (24) in appendix A showed TDOS and PDOS of normal Co_2MnGe at spin-down. For spin-down the major contributions of the VB is because of d-state of Co, d-state of

Mn and p-state of Ge. The major contributions of VB are from Co atom, then Mn atom and then a little contribution from Ge atom for normal Co_2MnGe compound.

Moreover, the major contribution of the CB is because of d-state of Co, d-state of Mn and both s and p-state of Ge. The major contributions of CB are from Co atom, then Mn atom and then a little contribution from Ge atom for normal Co_2MnGe compound.

Figures (23) and (24) in appendix A showed that normal Co_2MnGe Heusler compound has a half-metallic behavior, it's metallic at spin-up with zero band gap, and semi-conductor at spin-down with small band gap.

Figure (25) in appendix A showed TDOS and PDOS of inverse Co_2MnGe at spin-up. For spin-up the major contributions of the VB is because of d-state of Co, d-state of Mn and p-state of Ge. The major contributions of VB are from Co atom, then Mn atom and then a little contribution from Ge atom for inverse Co_2MnGe compound. But near fermi level the major contribution comes from Mn atom.

Furthermore, the major contribution of the CB is because of d-state of Mn, d-state of Co and both s and p-state of Ge. The major contributions of CB are from Mn atom, then Co atom and then a little contribution from Ge atom for inverse Co_2MnGe compound.

Figure (26) in appendix A showed TDOS and PDOS of invers Co_2MnGe at spin-down. For spin-down the major contributions of the VB is because of d-state of Co, d-state of Mn and p-state of Ge. The major contributions of VB are from Co atom, then Mn atom and then a little contribution from Ge atom for inverse Co_2MnGe compound.

On the other hand, the major contributions of the CB is because of d-state of Mn, d-state of Co and both s and p-state of Ge. The major contributions of CB are from Mn atom, then Co atom and then a little contribution from Ge atom for inverse Co_2MnGe compound. But near fermi level the major contribution comes from Co atom. But near fermi level the major contribution comes from Co atom.

Figures (21), (22), (25) and (26) in appendix A indicated the metallic behavior for both inverse Co2MnSi and Co_2MnGe Heusler compounds, both of inverse compounds have zero band gap in both spin-up and spin-down.

Previous studies have been studied the electronic properties for normal Heusler compounds Co_2MnSi and Co_2MnGe using GGA only. In addition to that in this study mBJ have been used, and the electronic properties for inverse Heusler compounds studied for the first time.

3.5 Elastic Properties

The bulk modulus (B), shear modulus (S), elastic constants (C_{ij}), Bugh ratio (B/S), Poisson's ratio (ν), Young's modulus (Y), and the anisotropic factor (A) of both normal and inverse Heusler compounds Co_2MnSi and Co_2MnGe were investigated in this study.

For cubic bulk alloys, we computed 3 symmetry elements, C_{11}, C_{12} and C_{44} to investigate the stability of compounds.

The mechanical stability Born–Huang criteria are as follows:(47–49)

$$\begin{aligned} &C11 > 0, \\ &C44 > 0, \\ &C11 + 2C12 > 0, \\ &C11 - C12 > 0, \\ &C11 > B > C12 \end{aligned} \tag{25}$$

The elastic constants for the normal Co_2MnSi Heusler compound are 317.387, 177.926 and 154.657 GPa for C_{11}, C_{12} and C_{44} consequently.

Also, for inverse Co_2MnSi Heusler compound these constants are 186.428, 184.205 and 107.202 GPa for C_{11}, C_{12} and C_{44} consequently.

For normal Co_2MnGe Heusler compound they are 281.542, 168.646 and 132.657 GPa for C_{11}, C_{12} and C_{44} consequently.

Moreover, for inverse Co_2MnGe Heusler compound they are 105.229, 161.111 and 98.077 GPa for C_{11}, C_{12} and C_{44} consequently.

According to the above mechanical stability conditions, regular Heusler alloys Co_2MnSi and Co_2MnGe and inverse Heusler alloy Co_2MnSi were mechanically stable, while the inverse Heusler alloys Co_2MnGe were mechanically unstable, as appeared in table (5).

Table 5

Elastic constants (C_{ii}) and bulk modulus (B) of normal and inverse Heusler compounds Co_2MnSi and Co_2MnGe

Compound	C_{11} (GPa)	C_{12} (GPa)	C_{44} (GPa)	B (GPa)
Normal Co_2MnSi	317.378	177.926	154.657	224.410
Inverse Co_2MnSi	186.428	184.205	10: 7.202	148.946
Normal Co_2MnGe	281.542	168.646	132.657	206.278
Inverse Co_2MnGe	105.229	161.111	98.077	142.484

Thereafter, the type of chemical bonds and the ductile behavior were investigated. The compounds have a Pugh ratio of B/S > 1.75 and Poisson's ratio ν > 0.26 had ductility, whereas others had brittle (50–53).

The Voigt shear modulus S_v, the Reuss shear modulus S_R, the Hill shear modulus S_H, and the bulk modulus B, have been determined within the following formulas (54–56):

$$S_v = \frac{1}{5}(C_{11} - C_{12} + 3C_{44}) \quad (26)$$

$$S_R = \frac{5C_{44}(C_{11}-C_{12})}{4C_{44}+3(C_{11}-C_{12})} \quad (27)$$

$$S_H = \frac{1}{2}(S_v + S_R) \quad (28)$$

$$B = \frac{1}{3}(C_{11} + 2C_{12}) \quad (29)$$

The nature of bonding has been investigated by the ν value. Compounds have covalent bonds if $\nu < 0.25$, while compounds have ionic bonds if $0.25 < \nu < 0.5$(48–50).

The ν value can be given by:

$$v = \frac{3B - 2S}{2(3B + S)} \quad (30)$$

Or

$$v = \frac{C_{12}}{C_{11} + C_{12}} \quad (31)$$

Young modulus (Y) (the ratio between stress and strain) and the anisotropic factor (A) are computed by the following:

$$Y = \frac{9SB}{S + 3B} \quad (32)$$

$$A = \frac{2C_{44}}{C_{11} - C_{12}} \quad (33)$$

The Shear modulus (S), Pugh ratio (B/S), Voigt Poisson's ratio (ν), and Young's modulus (Y) for normal and inverse Heusler compounds Co_2MnSi and Co_2MnGe are shown in table (6).

Table 6

The Shear modulus (S), Bugh ratio (B/S), Voigt Poisson's ratio (v), Young's modulus (Y) and anisotropic factor (A) for Heusler compounds

Compound	S (GPa)	B/S (GPa)	Y (GPa)	ν	A
Normal Co_2MnSi	112.337	1.998	288.819	0.285	3.221
inverse Co_2MnSi	33.751	4.414	95.448	0.414	96.448
Normal Co_2MnGe	94.156	2.191	245.167	0.302	2.350

B and S moduli determined the hardness of materials(57), whereas Y determined the stiffness of materials.

Moreover, the degree of anisotropy for the materials is measured by A(58). For an isotropic materials A = 1, otherwise, any other value show elastic anisotropy(59).

The anisotropic factor for normal Co_2MnSi Heusler compound, normal Co_2MnGe Heusler compound and inverse Co_2MnSi Heusler compound is 3.221, 2.350 and 96.448 respectively.

Table (5) shows that both normal and invers Heusler compounds Co_2MnSi and normal Heusler compound Co_2MnGe are satisfy the stability criteria and they classified mechanically stable, while inverse Heusler compound Co_2MnGe doesn't satisfy the stability conditions, and it's considered mechanically unstable.

According to anisotropic factor, both normal and inverse Heusler compounds Co_2MnSi and normal Heusler compound Co_2MnGe are elastic anisotropy.

B/S ratio for normal Co_2MnSi Heusler compound, normal Co_2MnGe Heusler compound and inverse Co_2MnSi Heusler compound is 1.998, 2.191 and 4.414 GPa respectively.

Voigt Poisson's ratio (ν) for normal Co_2MnSi Heusler compound, normal Co_2MnGe Heusler compound and inverse Co_2MnSi Heusler is 0.285, 0.302 and 0.414 respectively.

Table (6) indicates that both normal and invers Heusler compounds Co_2MnSi, and normal Heusler compound Co_2MnGe are ductile since $B/S > 1.75$ and $\nu > 0.26$.

According to ν values table (6) indicates that both normal and inverse Heusler compounds Co_2MnSi and normal Heusler compound Co_2MnGe have ionic bonds.

Chapter Four

Discussions and Conclusions

In this study structural, electronic, magnetic and elastic properties of both normal and inverse Co_2MnSi and Co_2MnGe full Heusler compounds have been determined.

Lattice constant (a) have been computed by Murnaghan's equation of state (EOS). For normal Co_2MnSi, normal Co_2MnGe, inverse Co_2MnSi and inverse Co_2MnGe lattice constant was 5.6347, 5.7351, 5.6459 and 5.7528, respectively.

New results are in good agreement with earlier experimental and theoretical results for normal compounds, but for invers compounds there aren't previous studies.

The band structure studied found that both normal Co_2MnSi and Co_2MnGe full Heusler compounds behave as half-metallic with direct band gap at spin-down. These compounds behave as metallic at spin-up, and semiconductor at spin-down. While inverse Co_2MnSi and Co_2MnGe full Heusler compounds behave as metallic, with no band gap.

The mBJ approximation enhances the energy band gap for both normal Co_2MnSi and Co_2MnGe full Heusler compounds in spin-down by 79.609 % and 168.339 % for normal Co_2MnSi and normal Co_2MnGe.

New results are in good agreement with earlier results for normal compounds by GGA. The mBJ approximation and invers compounds haven't studied before yet.

The total density of state cleared that the major contributions of the valence and conducting band come from Co atom, then Mn atom and then a little contribution from Si at both spin-up and spin-down of normal Co_2MnSi full Heusler compound.

For normal Co_2MnGe full Heusler compound, the major contributions for the valence and conducting band are from Co atom, then Mn atom and then a little contribution from Ge at both spin-up and spin-down.

Moreover, for inverse Co_2MnSi full Heusler compound the major contributions of the valence band are from Co atom, then Mn atom and then a little contribution from Si at both spin-up and spin-down, but for conducting band the major contributions are from

Mn atom, then Co atom, then a little contribution from Si atom at both spin-up and spin-down.

Furthermore, for inverse Co_2MnGe full Heusler compound the major contributions of the valence and conducting band are from Co atom, then Mn atom and then a little contribution from Ge at both spin-up and spin-down, but for conducting band the major contributions are from Mn atom, then Co atom, then a little contribution from Ge atom at both spin-up and spin-down..

The calculated total magnetic moments for normal Co_2MnSi, normal Co_2MnGe, inverse Co_2MnSi and inverse Co_2MnGe are 4.99382, 4.96698, 4.31954 and 4.97734 μ_B respectively by GGA. These values indicate that all of these compounds are ferromagnetic material.

The calculated total magnetic moments by mBJ approximation are 4.99999, 4.99994, 4.78272 and 6.13948 μ_B for normal Co_2MnSi, normal Co_2MnGe, inverse Co_2MnSi and inverse Co_2MnGe respectively. These values indicate that all of these compounds are ferromagnetic material.

Our new calculations have a good agreement with previous results for both normal Co_2MnSi, normal Co_2MnGe by GAA. The inverse compounds Co_2MnSi and Co_2MnGe and the mBJ approximation studied for the first time in this research.

The elastic properties indicate that normal Co_2MnSi, normal Co_2MnGe and inverse Co_2MnSi Heusler compounds are mechanically stable, while inverse Co_2MnGe Heusler compound is mechanically unstable.

The anisotropic factor for normal Co_2MnSi, normal Co_2MnGe and inverse Co_2MnSi is 3.221, 2.350 and 96.448 respectively. These values indicate that all of these compounds are elastic anisotropy.

B/S results for normal Co_2MnSi, normal Co_2MnGe and inverse Co_2MnSi are 1.998, 2.191 and 4.414 respectively. According to these results both normal and invers Heusler compounds Co_2MnSi, and normal Heusler compound Co_2MnGe are ductile.

Poisson’s ratio (ν) for normal Co_2MnSi, normal $Co_2MnGe$and inverse Co_2MnSi is 0.285, 0.302 and 0.414 respectively. These results show that both normal and inverse Co_2MnSi and normal Co_2MnGe have ionic bonds.

This study is considered as a hot topic since the importance of this study lies in the totally different behavior in spin-up and spin-down bands for these normal Heusler compounds. The spin-up electrons behave metallically, while the spin-down electrons are semiconducting. They are classified half-metallic ferromagnets material.

The half-metallic ferromagnetic materials are identified as an extremely exiting material for spintronic and magneto-electronics.

List of Abbreviations

Abbreviation	Meaning
FP-LAPW	Full Potential Linearized Augmented Plane Wave
FCC	Face-centered cubic
BOA	Born-Oppenheimer Approximation
DFT	Density Functional Theory
LDA	Local Density Approximation
GGA	Generalized Gradient Approximation
APW	Augmented Plane Wave
LAPW	Linearized Augmented Plane Wave
mBJ	Modified Becke-Johnson
BS	Band Structure
DOS	Density Of State
TDOS	Total Density of State
PDOS	Partial Density of State
HM	Half-Metallic
SE	Schrödinger Equation
KS	Kohn-Sham
CB	Conduction Band
VB	Valence Band

References

1. De Groot RA, Mueller FM, van Engen PG v, Buschow KHJ. New class of materials: half-metallic ferromagnets. Phys Rev Lett. 1983;50(25):2024.

2. Berrahal M, Bentouaf A, Rached H, Mebsout R, Aissa B. Investigation of Ruthenium based Full-Heusler compound for thermic, spintronics and thermoelectric applications: DFT computation. Mater Sci Semicond Process. 2021;134:106047.

3. Patel PD, Pandya JB, Shinde SM, Gupta SD, Narayan S, Jha PK. Investigation of Full-Heusler compound Mn2MgGe for magnetism, spintronics and thermoelectric applications: DFT study. Computational Condensed Matter. 2020;23:e00472.

4. Elphick K, Frost W, Samiepour M, Kubota T, Takanashi K, Sukegawa H, et al. Heusler alloys for spintronic devices: review on recent development and future perspectives. Sci Technol Adv Mater. 2021;22(1):235–71.

5. Arshad H, Zafar M, Ahmad S, Rizwan M, Khan MI, Gillani SSA, et al. Theoretical study of structural, electronic and magnetic properties of equiatomic quaternary CoPdCrZ (Z= Si, Ge, P) Heusler alloys. Modern Physics Letters B. 2019;33(31):1950389.

6. Elphick K, Frost W, Samiepour M, Kubota T, Takanashi K, Sukegawa H, et al. Heusler alloys for spintronic devices: review on recent development and future perspectives. Sci Technol Adv Mater. 2021;22(1):235–71.

7. Ahmad A, Das AK, Srivastava SK. Competition of L2 1 and XA ordering in Fe 2 CoAl Heusler alloy: a first-principles study. Eur Phys J B. 2020;93:1–7.

8. Galanakis I, Mavropoulos P, Dederichs PH. Electronic structure and Slater–Pauling behaviour in half-metallic Heusler alloys calculated from first principles. J Phys D Appl Phys. 2006;39(5):765.

9. Dai X, Liu G, Chen L, Chen J, Wu G. Mn2 CoSb compound: Structural, electronic, transport and magnetic properties. Solid State Commun. 2006;140(11–12):533–7.

10. Liu GD, Dai XF, Liu HY, Chen JL, Li YX, Xiao G, et al. Mn 2 co z (z= al, ga, in, si, ge, sn, sb) compounds: Structural, electronic, and magnetic properties. Phys Rev B. 2008;77(1):014424.

11. Bayar E, Kervan N, Kervan S. Half-metallic ferrimagnetism in the Ti2CoAl Heusler compound. J Magn Magn Mater. 2011;323(23):2945–8.

12. Fang QL, Zhang JM, Xu KW, Ji V. Electronic structure and magnetism of Ti2FeSi: A first-principles study. J Magn Magn Mater. 2013;345:171–5.

13. Jia HY, Dai XF, Wang LY, Liu R, Wang XT, Li PP, et al. Doping effect on electronic structures and band gap of inverse Heusler compound: Ti2CrSn. J Magn Magn Mater. 2014;367:33–9.

14. Kervan N, Kervan S. A first-principle study of half-metallic ferrimagnetism in the Ti2CoGa Heusler compound. J Magn Magn Mater. 2012;324(4):645–8.

15. Birsan A, Palade P, Kuncser V. Prediction of half metallic properties in Ti2CoSi Heusler alloy based on density functional theory. J Magn Magn Mater. 2013;331:109–12.

16. Yamamoto M, Marukame T, Ishikawa T, Matsuda K i, Uemura T, Arita M. Fabrication of fully epitaxial magnetic tunnel junctions using cobalt-based full-Heusler alloy thin film and their tunnel magnetoresistance characteristics. J Phys D Appl Phys. 2006;39(5):824.

17. Kämmerer S, Thomas A, Hütten A, Reiss G. Co 2 Mn Si Heusler alloy as magnetic electrodes in magnetic tunnel junctions. Appl Phys Lett. 2004;85(1):79–81.

18. Okamura S, Miyazaki A, Sugimoto S, Tezuka N, Inomata K. Large tunnel magnetoresistance at room temperature with a Co 2 FeAl full-Heusler alloy electrode. Appl Phys Lett. 2005;86(23):232503.

19. Brown PJ, Ziebeck KRA, Huntley JM. Magnetisation density in the Heusler alloy Fe2MnSi. J Magn Magn Mater. 1985;50(2):169–77.

20. Fujii S, Ishida S, Asano S. A half-metallic band structure and Fe2MnZ (Z= Al, Si, P). J Physical Soc Japan. 1995;64(1):185–91.

21. Luo H, Zhu Z, Ma L, Xu S, Liu H, Qu J, et al. Electronic structure and magnetic properties of Fe2YSi (Y= Cr, Mn, Fe, Co, Ni) Heusler alloys: a theoretical and experimental study. J Phys D Appl Phys. 2007;40(22):7121.

22. Ishida S, Nagatomo D, Fujii S, Asano S. Theoretical search of spintronic material in Fe2 (Cr1− xMnx) Si and (Fe1− xCox) 2MnSi. Mater Trans. 2008;49(1):114–9.

23. Saito T, Katayama T, Ishikawa T, Yamamoto M, Asakura D, Koide T, et al. Interface structure of half-metallic Heusler alloy Co 2 MnSi thin films facing an MgO tunnel barrier determined by x-ray magnetic circular dichroism. Physical Review B—Condensed Matter and Materials Physics. 2010;81(14):144417.

24. Itoh H, Honda S, Inoue J. Electronic Structure and Spin-Injection of Co-Based Heusler Alloy/Semiconductor Junctions. Key Eng Mater. 2011;470:54–9.

25. Hamad B, Hu Q. The effect of defects on the electronic and magnetic properties of Fe2MnSi Heusler alloy. physica status solidi (b). 2011;248(12):2893–8.

26. Shigeta I, Urakawa S, Ito M, Hiroi M. Magnetization and spin polarization of Co2− xFexMnSi Heusler alloys. In: Journal of Physics: Conference Series. IOP Publishing; 2012. p. 032082.

27. Pedro SS, Caraballo Vivas RJ, Andrade VM, Cruz C, Paixao LS, Contreras C, et al. Effects of Ga substitution on the structural and magnetic properties of half metallic Fe2MnSi Heusler compound. J Appl Phys. 2015;117(1).

28. Hiroi M, Ishikuma S, Shigeta I, Koyama K, Kondo A, Kindo K, et al. Magnetization and magnetic phase diagram of Heusler compounds Fe3− y (Mn1− xVx) ySi (y= 1 and 1.5). In: Journal of Physics: Conference Series. IOP Publishing; 2018. p. 012099.

29. Hiroi M, Nonoyama T, Adachi G, Shigeta I, Manaka H, Terada N. Magnetic properties of Heusler compound Fe1. 3Mn1. 7Si. In: Journal of Physics: Conference Series. IOP Publishing; 2018. p. 012098.

30. El Krimi Y, Masrour R, Jabar A, Labidi S, Bououdina M, Ellouze M. Structural, electronic, magnetic and thermoelectric properties of Full-Heusler Fe2MnSi: Ab initio calculations. Results Phys. 2020;18:103252.

31. Wu C, Zheng W, Si N, Li C, Zhang Y, Jiang W. Electronic structure, magnetic properties, and elastic properties of full-Heusler alloys Cr2-xFexMnSi (x= 0, 1, and 2). Europhys Lett. 2021;133(5):58002.

32. Ishida S, Masaki T, Fujii S, Asano S. Theoretical search for half-metalliic films of Co2MnZ (Z□ Si, Ge). Physica B Condens Matter. 1998;245(1):1–8.

33. Bhatt H, Mukadam MD, Meena SS, Yusuf SM. Fe2-x Co x MnSi (x= 0, 1 and 2) Heusler alloys: Structural, magnetic and atomic site disorder properties. In: AIP Conference Proceedings. AIP Publishing LLC; 2015. p. 130048.

34. Aguilera-Granja F, Aguilera-del-Toro RH, Morán-López JL. A first principles systematic study of the structural, electronic, and magnetic properties of Heusler X2MnZ with X= Fe, Co, Ni, Cu, Ru, Rh, Pd, Ag, Pt, Au and Z= Al, Si, Ga, Ge, In and Sn. Mater Res Express. 2019;6(10):106118.

35. Pradines B, Calmels L, Arras R. Robustness of the Half-Metallicity at the Interfaces in Co 2 Mn Si-Based All-Full-Heusler-Alloy Spintronic Devices. Phys Rev Appl. 2021;15(3):034009.

36. Cottenier S. Density Functional Theory and the family of (L) APW-methods: a step-by-step introduction. Instituut voor Kern-en Stralingsfysica, KU Leuven, Belgium. 2002;4(0):41.

37. Schwarz K. DFT calculations of solids with LAPW and WIEN2k. J Solid State Chem. 2003;176(2):319–28.

38. Blaha P, Schwarz K, Madsen GKH, Kvasnicka D, Luitz J. wien2k. An augmented plane wave+ local orbitals program for calculating crystal properties. 2001;60(1):7–12.

39. Born M, Oppenheimer R. On the quantum theory of molecules. In: Quantum Chemistry: Classic Scientific Papers. World Scientific; 2000. p. 1–24.

40. Schrödinger E. An undulatory theory of the mechanics of atoms and molecules. Uspekhi Fizicheskikh Nauk. 1927;7(3):176–201.

41. Sholl DS, Steckel JA. Density functional theory: a practical introduction. John Wiley & Sons; 2022. 1–14 p.

42. Kohn W, Sham LJ. Self-consistent equations including exchange and correlation effects. Physical review. 1965;140(4A):A1133.

43. Ziesche P, Kurth S, Perdew JP. Density functionals from LDA to GGA. Comput Mater Sci. 1998;11(2):122–7.

44. Tran F, Blaha P, Schwarz K. Band gap calculations with Becke–Johnson exchange potential. Journal of Physics: Condensed Matter. 2007;19(19):196208.

45. Jamal M, Bilal M, Ahmad I, Jalali-Asadabadi S. IRelast package. J Alloys Compd. 2018;735:569–79.

46. Paudel R, Zhu J. Investigation of half-metallicity and magnetism of (Ni/Pd/Ru) ZrTiAl quaternary Heusler alloys for spintronic applications. Physica B Condens Matter. 2019;557:45–51.

47. Born M, Huang K, Lax M. Dynamical Theory of Crystal Lattices. Am J Phys. 1955;23(7):474.

48. Gupta Y, Sinha MM, Verma SS. Exploring the structural, elastic, lattice dynamical stability and thermoelectric properties of semiconducting novel quaternary Heusler alloy LiScPdPb. J Solid State Chem. 2021;304:122601.

49. Abu-Jafar M, Dayton-Oxland R, Jaradat R, Mousa AA, Khenata R. Structural, electronic, mechanical and elastic properties of Scandium Chalcogenides by first-principles calculations. Phase Transitions. 2020;93(8):773.

50. Pugh SF. XCII. Relations between the elastic moduli and the plastic properties of polycrystalline pure metals. The London, Edinburgh, and Dublin Philosophical Magazine and Journal of Science. 1954;45(367):823.

51. Abu-Jafar MS, Leonhardi V, Jaradat R, Mousa AA, Al-Qaisi S, Mahmoud NT, et al. Structural, electronic, mechanical, and dynamical properties of scandium carbide. Results Phys. 2021;21:103804.

52. Cheriet A, Khenchoul S, Aissani L, Lagoun B, Zaabat M, Alhussein A. First-principles calculations to investigate structural, magnetic, electronic and elastic properties of full-Heusler alloys Co2MB (M= V, Mn). Solid State Commun. 2021;337:114426.

53. Abada A, Marbouh N, Bentayeb A. First-principles calculations to investigate structural, elastic, electronic and magnetic properties of novel d0 half metallic half Heusler alloys XSrB (X= Be, Mg). Intermetallics (Barking). 2022;140:107392.

54. Voigt W. Ueber die Beziehung zwischen den beiden Elasticitätsconstanten isotroper Körper. Ann Phys. 1889;274(12):573.

55. Reuss A. Berechnung der Fließgrenze von Mischkristallen auf Grund der Plastizitätsbedingung für Einkristalle. Zeitschrift Angewandte Mathematik und Mechanik. 1929;9(1):49.

56. Hill R. The elastic behaviour of a crystalline aggregate. Proceedings of the Physical Society Section A. 1952;65(5):349.

57. Teter DM. Computational alchemy: the search for new superhard materials. MRS Bull. 1998;23(1):22.

58. Zener C. Elasticity and an Elasticity of Metals. University of Chicago Press, Chicago. 1948;

59. Ravindran P, Fast L, Korzhavyi PA, Johansson B, Wills J, Eriksson O. Density functional theory for calculation of elastic properties of orthorhombic crystals: Application to TiSi 2. J Appl Phys. 1998;84(9):4891.

Appendices

Appendix A

DOS Figures

Figure 11

TDOS and PDOS of spin-up for normal Co_2MnSi compound using GGA

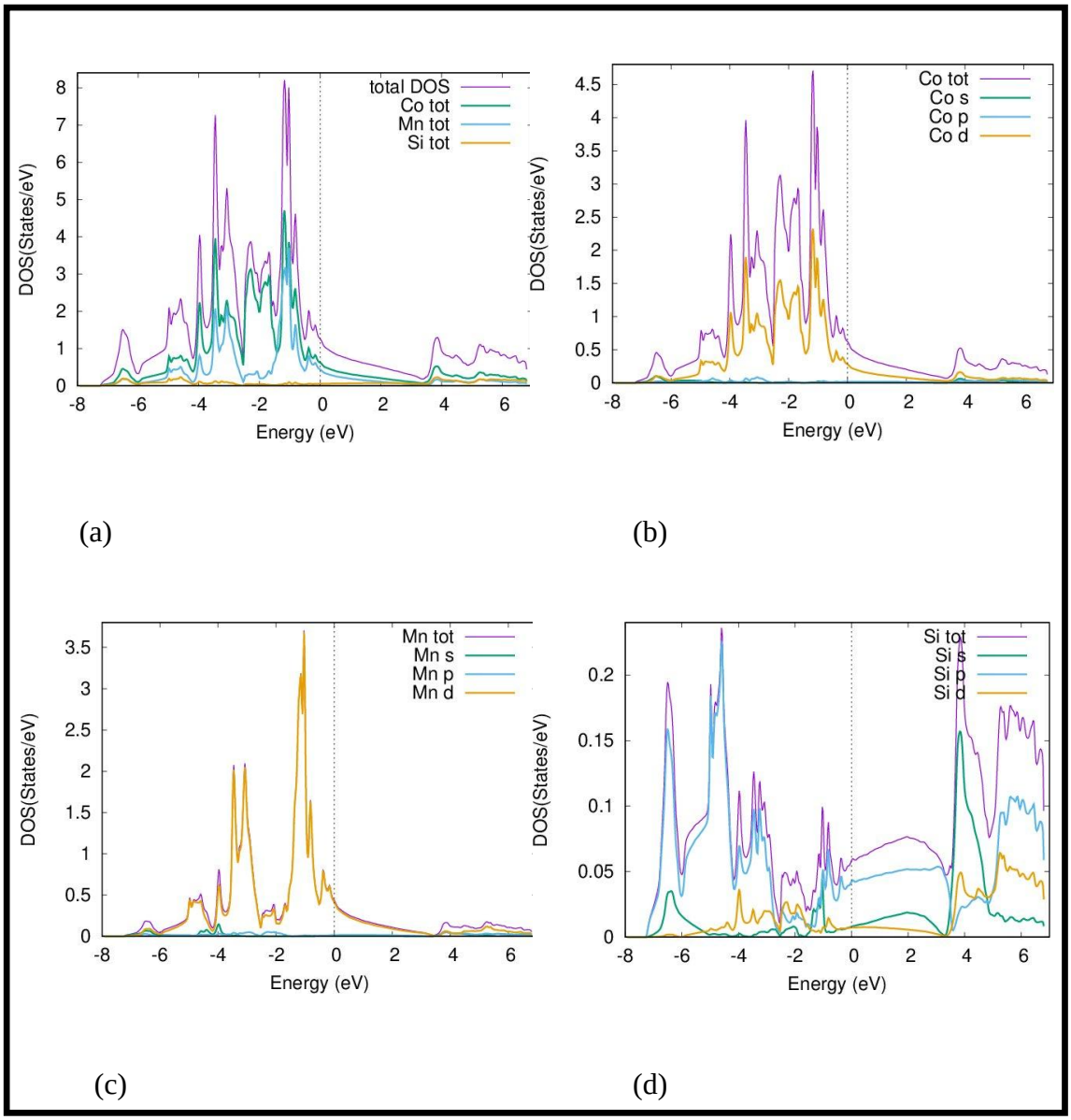

Note: (a) TDOS (b) PDOS for Co atom, (c) PDOS for Mn atom, (d) PDOS for Si atom.

Figure 12

TDOS and PDOS of spin-down for normal Co_2MnSi compound using GGA

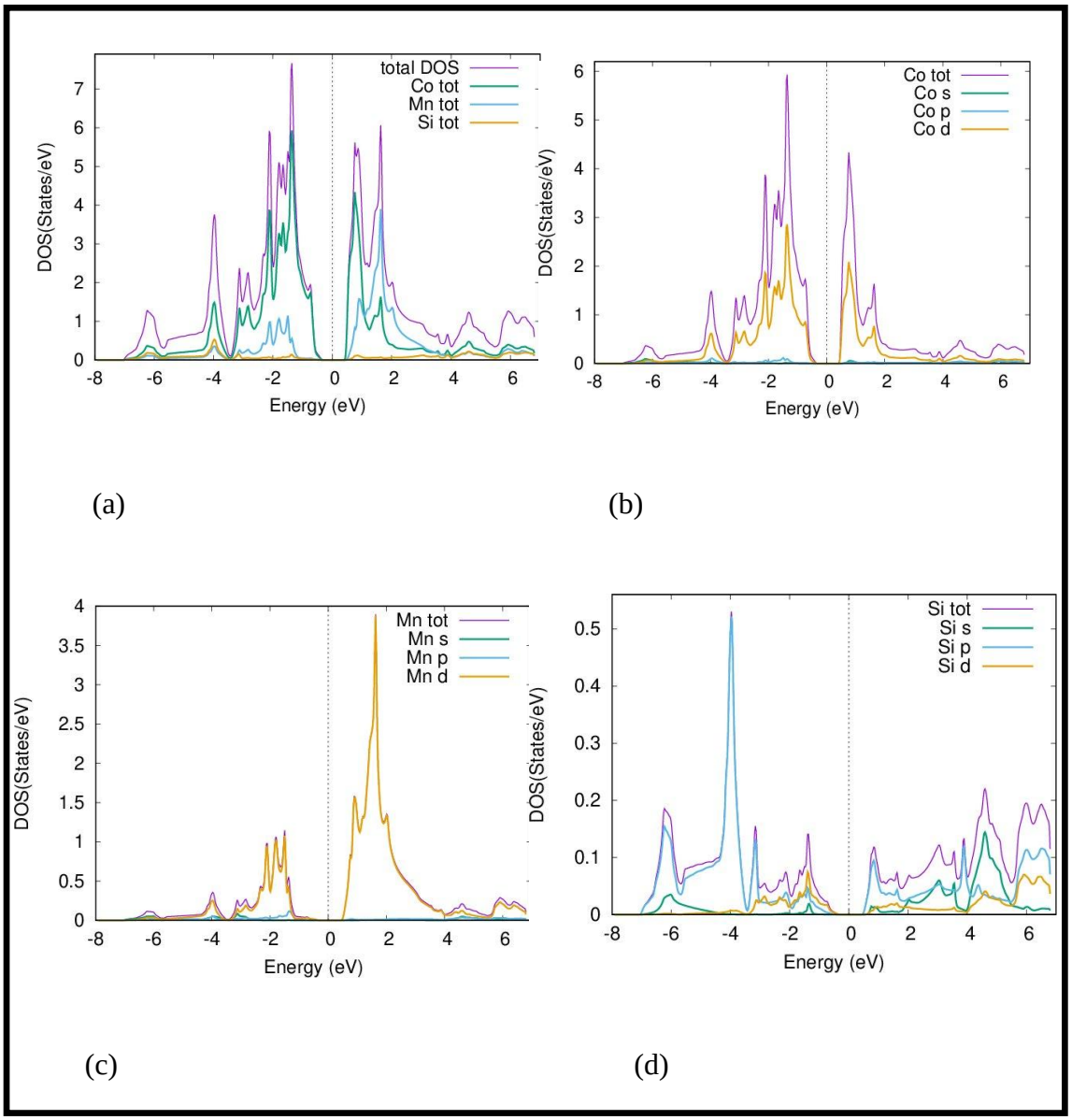

Note: (a) TDOS (b) PDOS of Co atom, (c) PDOS of Mn atom, (d) PDOS of Si atom.

Figure 13

TDOS and PDOS of spin-up for inverse Co_2MnSi compound using GGA

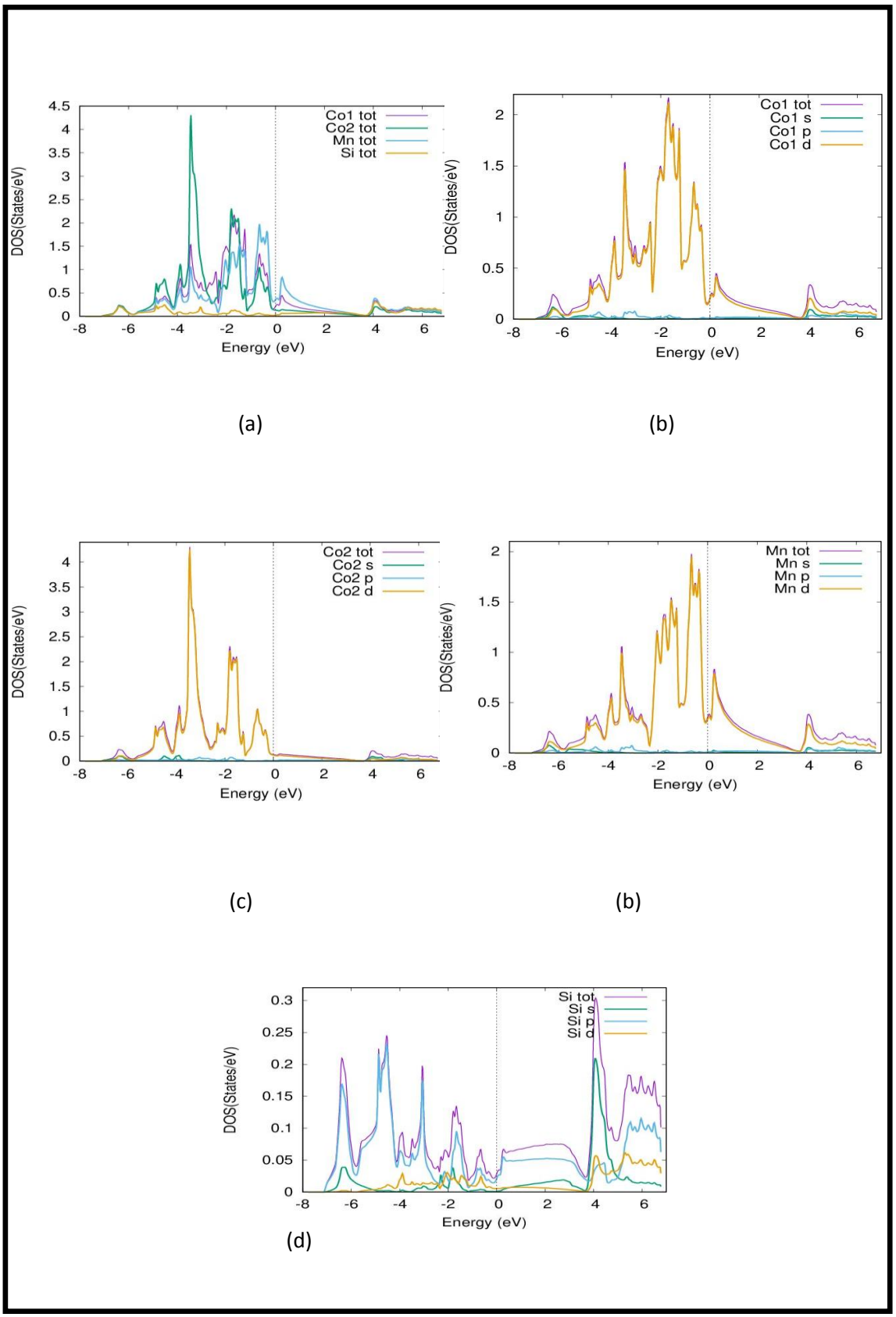

Note: (a) TDOS (b) PDOS for Co_1 atom, (c) PDOS for Co_2 atom, (d) PDOS for Mn atom, (e) PDOS for Si atom.

Figure 14

TDOS and PDOS of spin-down for inverse Co_2MnSi compound using GGA

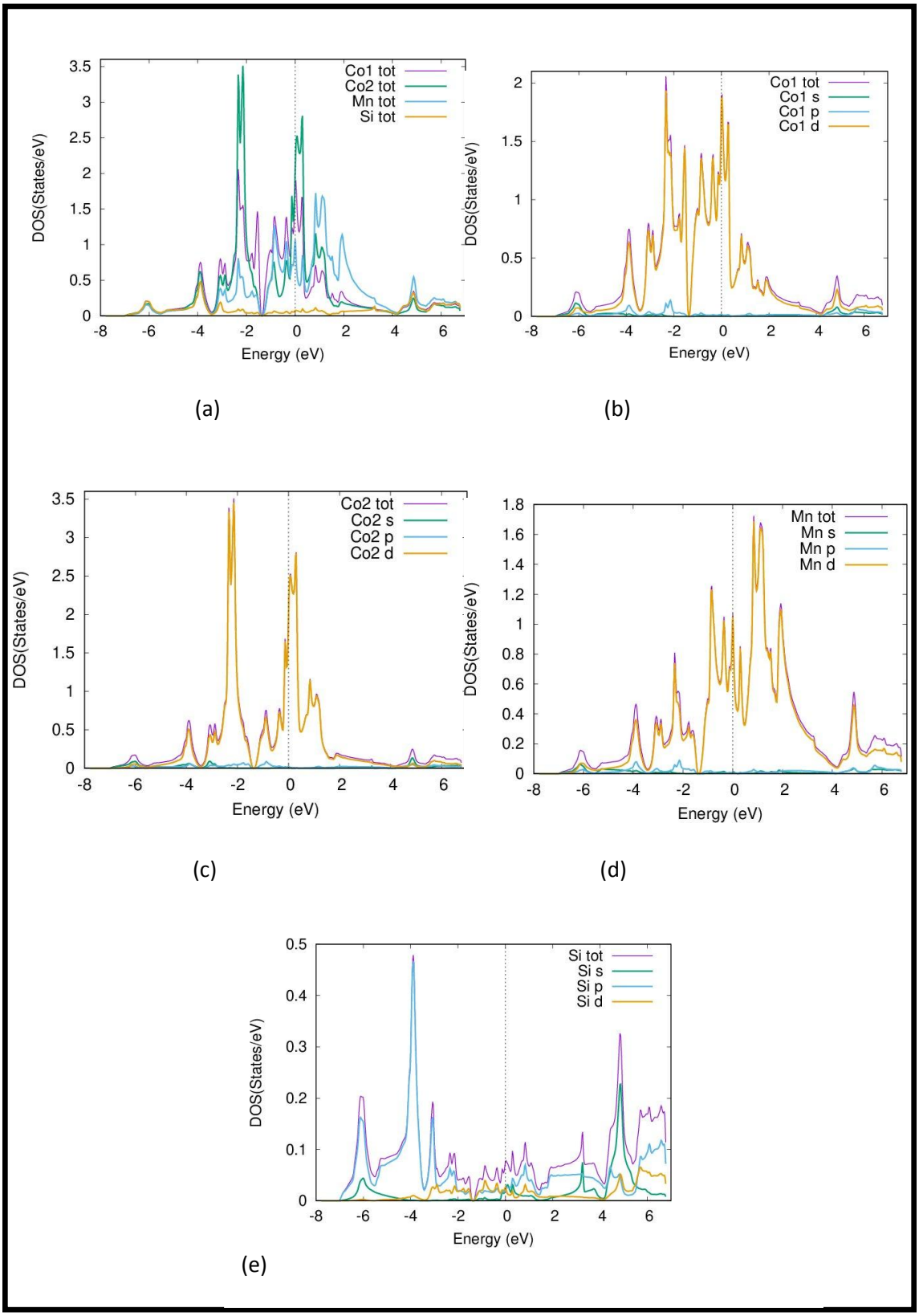

Note: (a) TDOS (b) PDOS for Co_1 atom, (c) PDOS for Co_2 atom, (d) PDOS for Mn atom, (e) PDOS for Si atom.

Figure 15

TDOS and PDOS of spin-up for normal Co_2MnGe compound using GGA

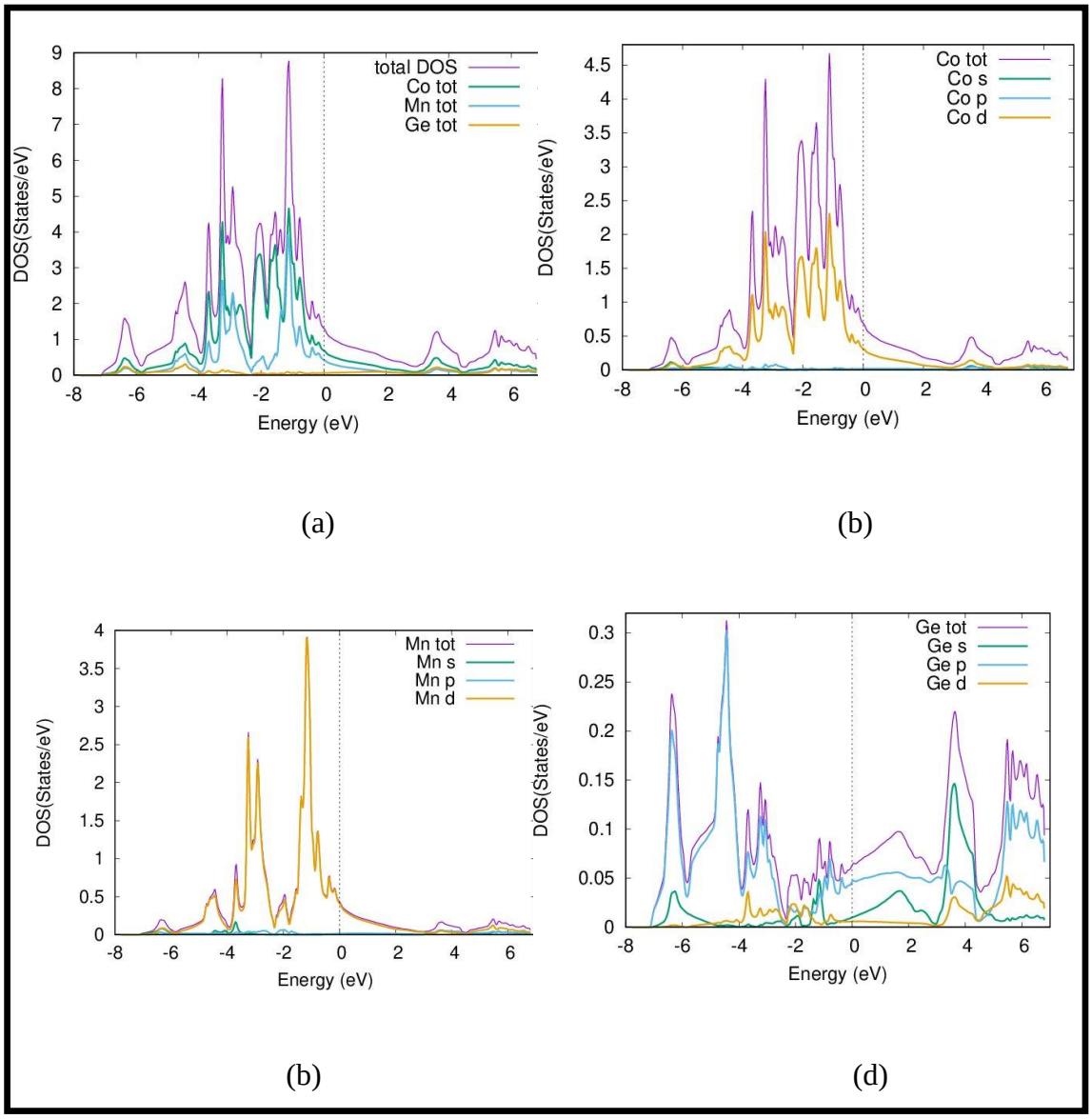

Note: (a) TDOS (b) PDOS for Co atom, (c) PDOS for Mn atom, (d) PDOS for Ge atom.

Figure 16

TDOS and PDOS of spin-down for normal Co_2MnGe compound using GGA

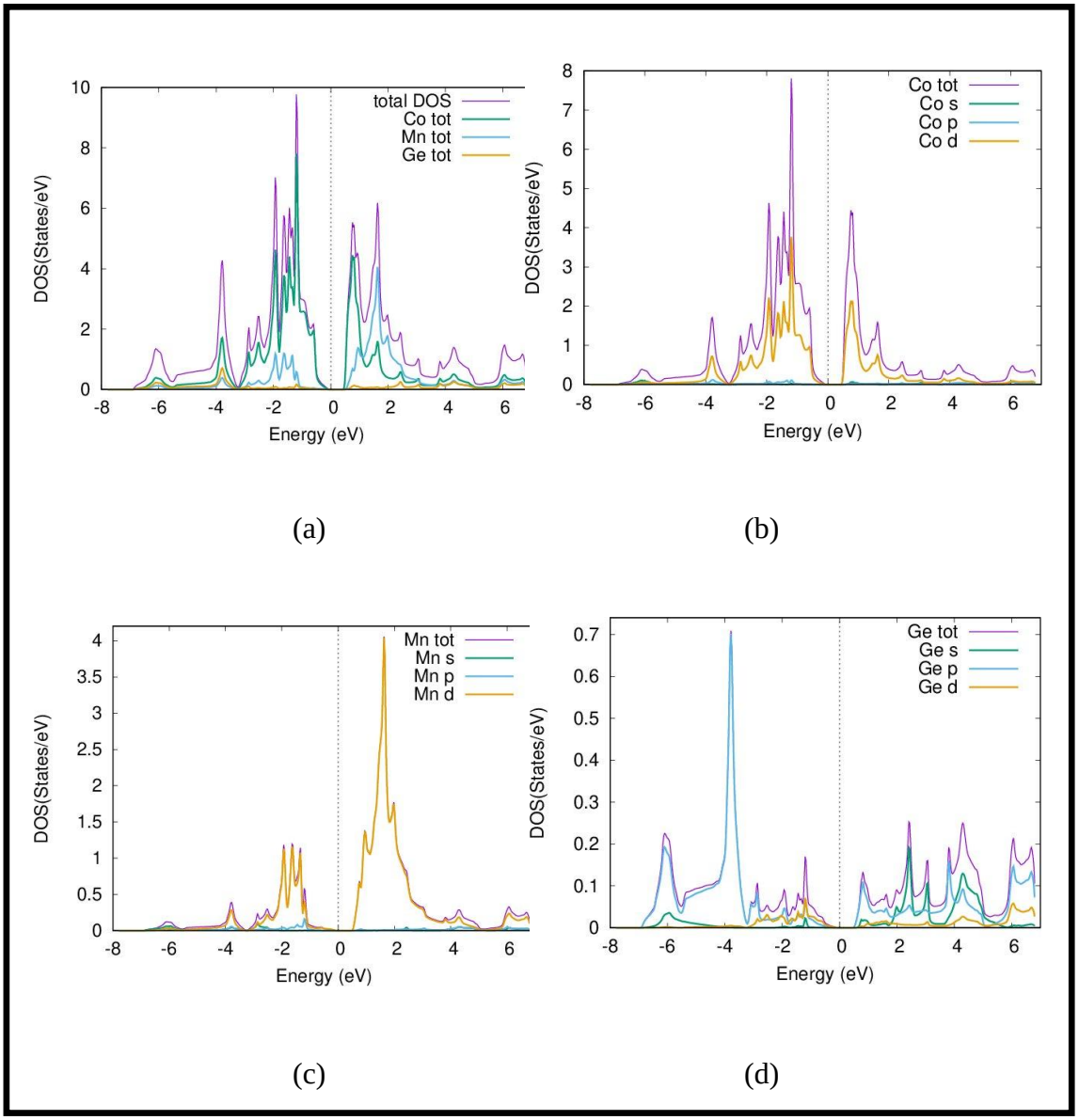

Note: (a) TDOS (b) PDOS for Co atom, (c) PDOS for Mn atom, (d) PDOS for Ge atom.

Figure 17

TDOS and PDOS of spin-up for inverse Co_2MnGe compound using GGA

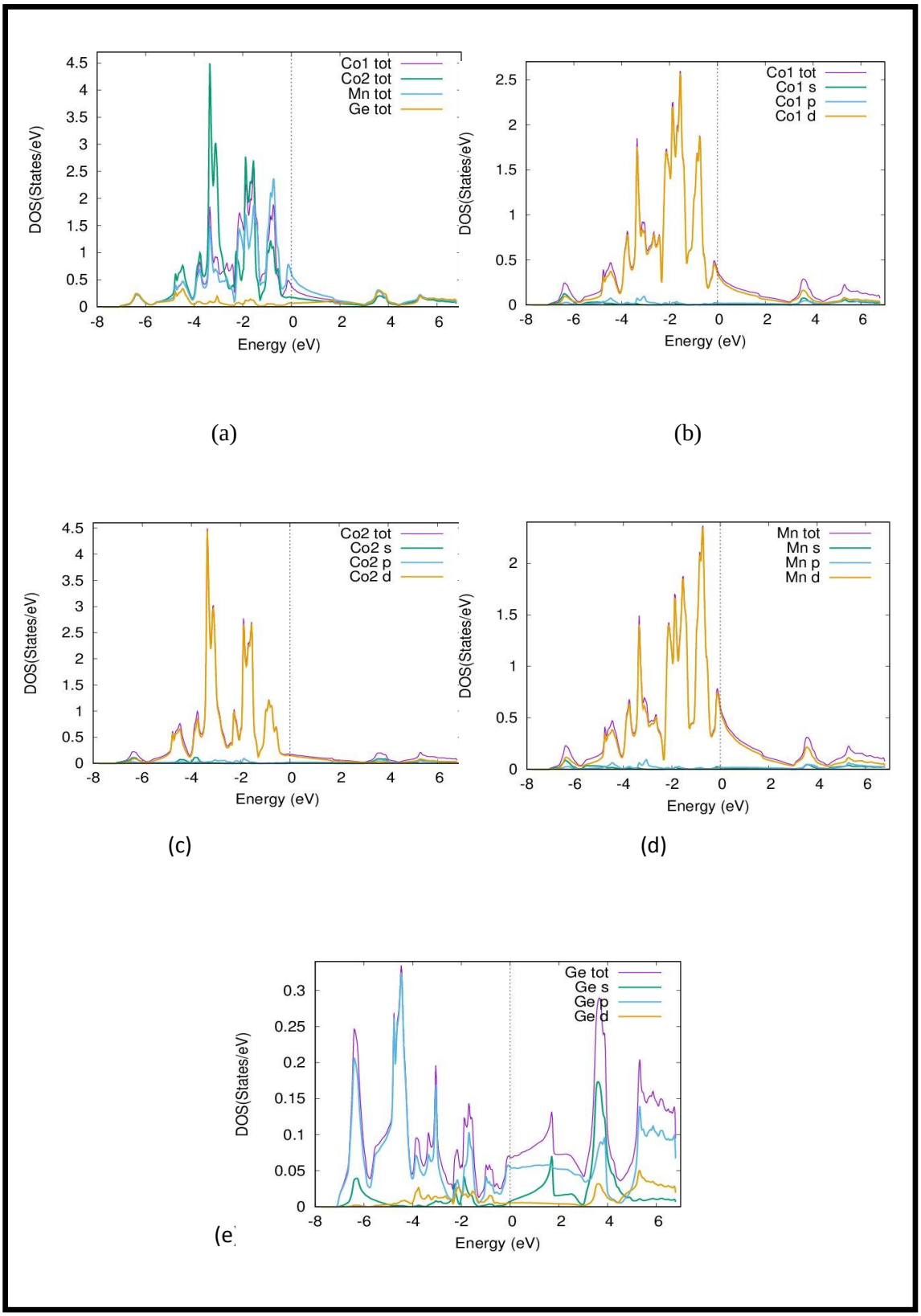

Note: (a) TDOS (b) PDOS for Co_1 atom, (c) PDOS for Co_2 atom, (d) PDOS for Mn atom, (e) PDOS for Ge atom.

Figure 18

TDOS and PDOS of spin-down for inverse Co_2MnGe compound using GGA

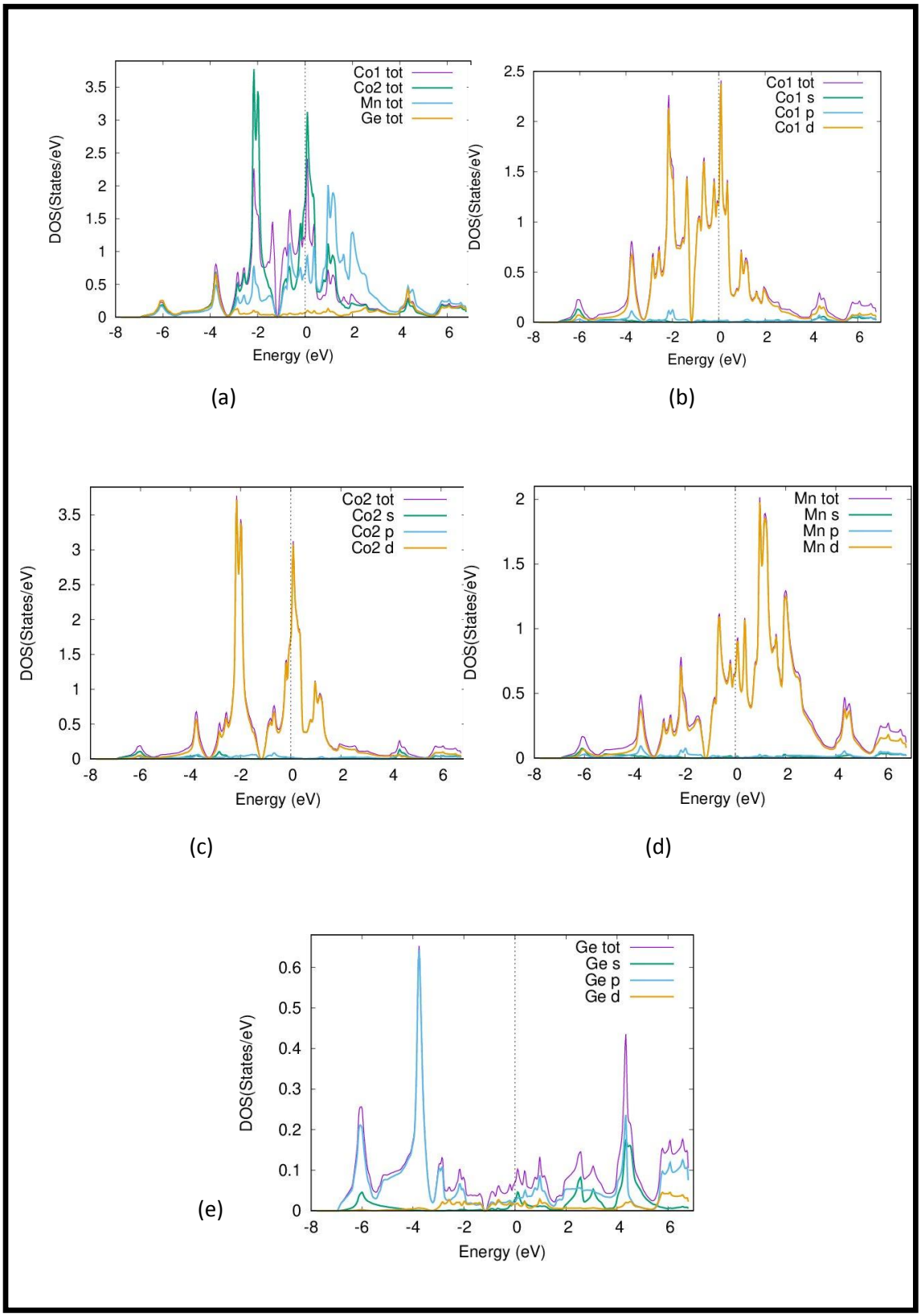

Note: (a) TDOS (b) PDOS for Co_1 atom, (c) PDOS for Co_2 atom, (d) PDOS for Mn atom, (e) PDOS for Ge atom.

Figure 19

TDOS and PDOS of spin-up for normal Co_2MnSi compound using mBJ

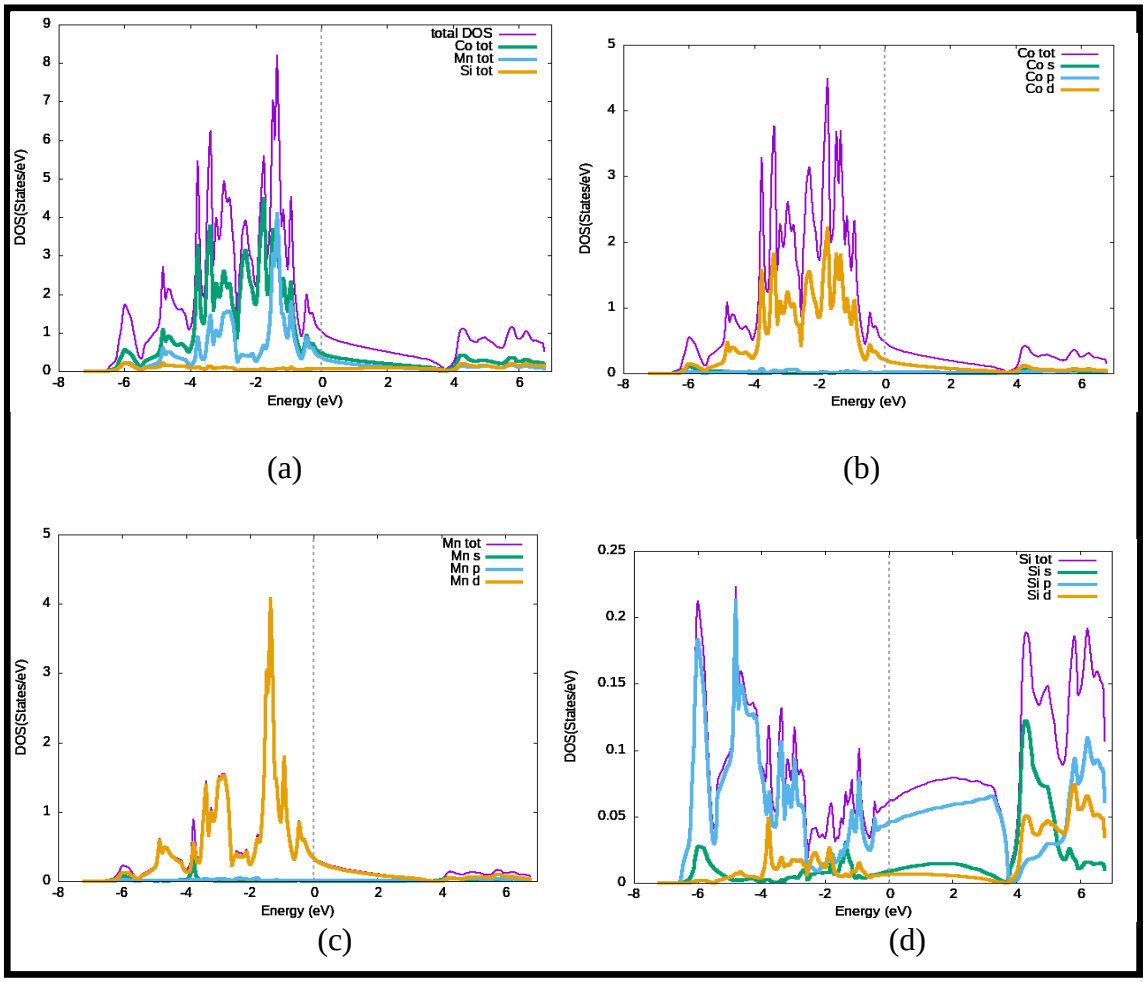

Note: (a) TDOS (b) PDOS for Co atom, (c) PDOS for Mn atom, (d) PDOS for Si atom.

Figure 20

TDOS and PDOS of spin-down for normal Co_2MnSi compound using mBJ

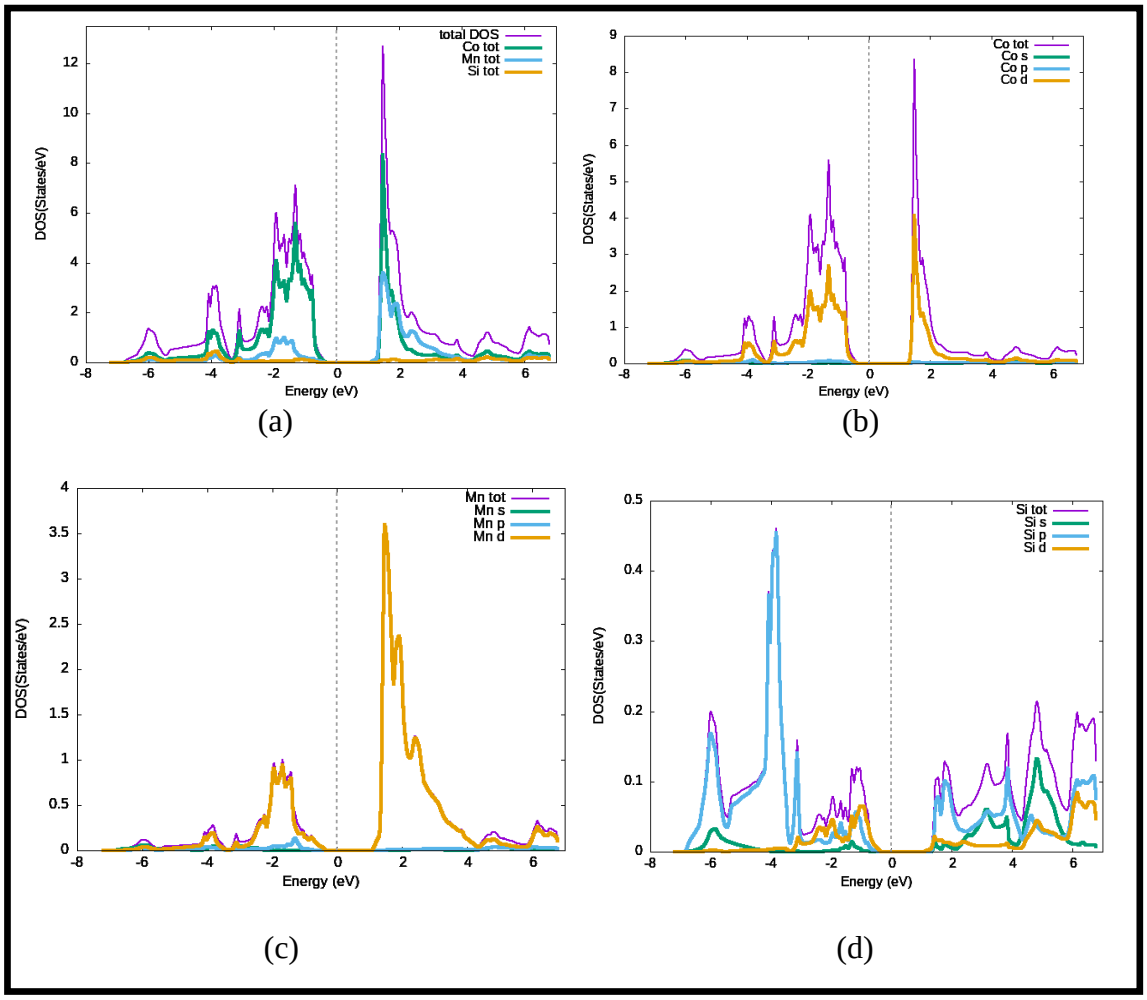

Note: (a) TDOS (b) PDOS for Co atom, (c) PDOS for Mn atom, (d) PDOS for Si atom.

Figure 21

TDOS and PDOS of spin-up for inverse Co_2MnSi compound using mBJ

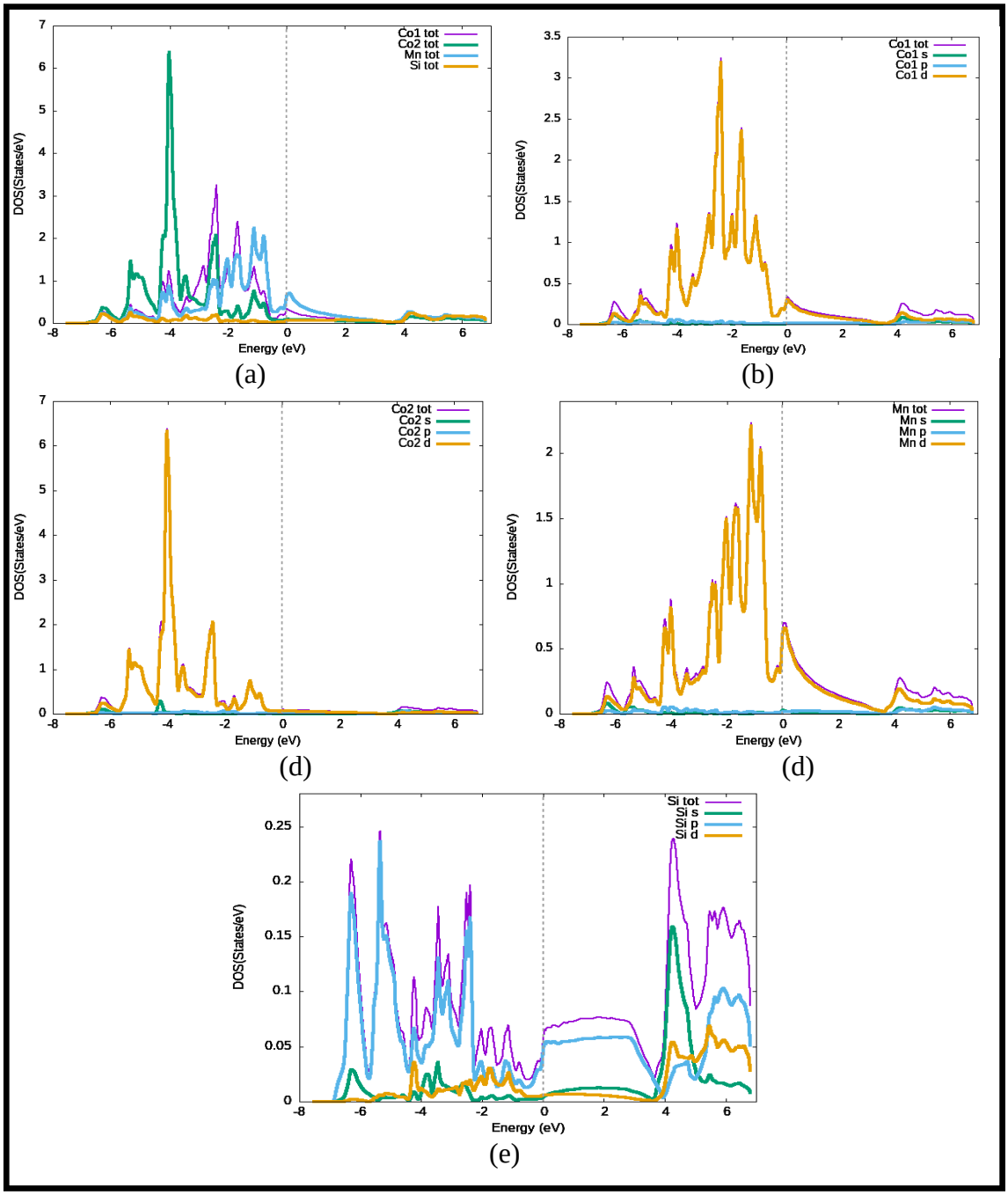

Note: (a) TDOS (b) PDOS for Co_1 atom, (c) PDOS for Co_2 atom, (d) PDOS for Mn atom, (e) PDOS for Si atom.

Figure 22

TDOS and PDOS of spin-down for inverse Co_2MnSi compound using mBJ

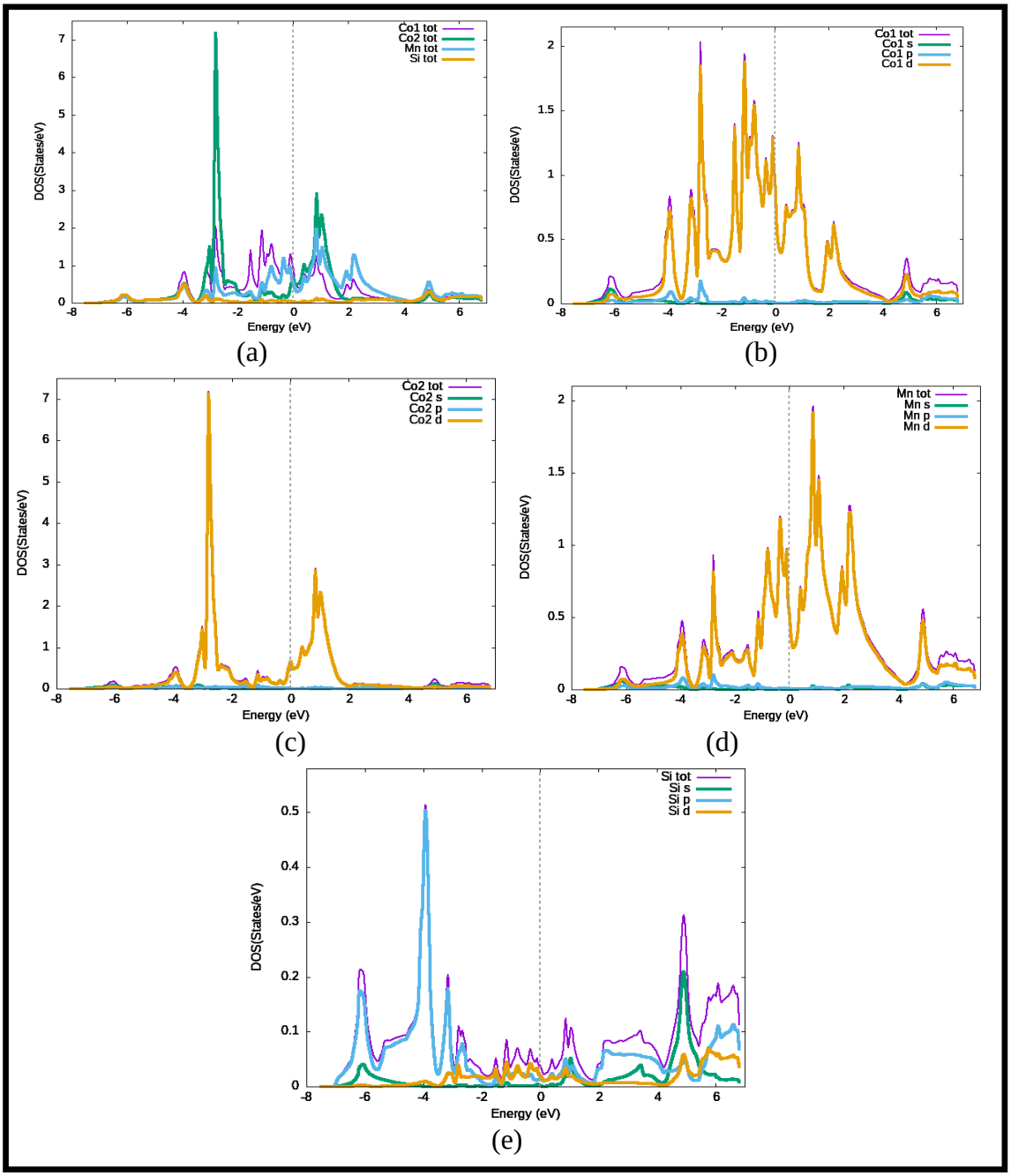

Note: (a) TDOS (b) PDOS for Co_1 atom, (c) PDOS for Co_2 atom, (d) PDOS for Mn atom, (e) PDOS for Si atom.

Figure 23

TDOS and PDOS of spin-up for normal Co_2MnGe compound using mBJ

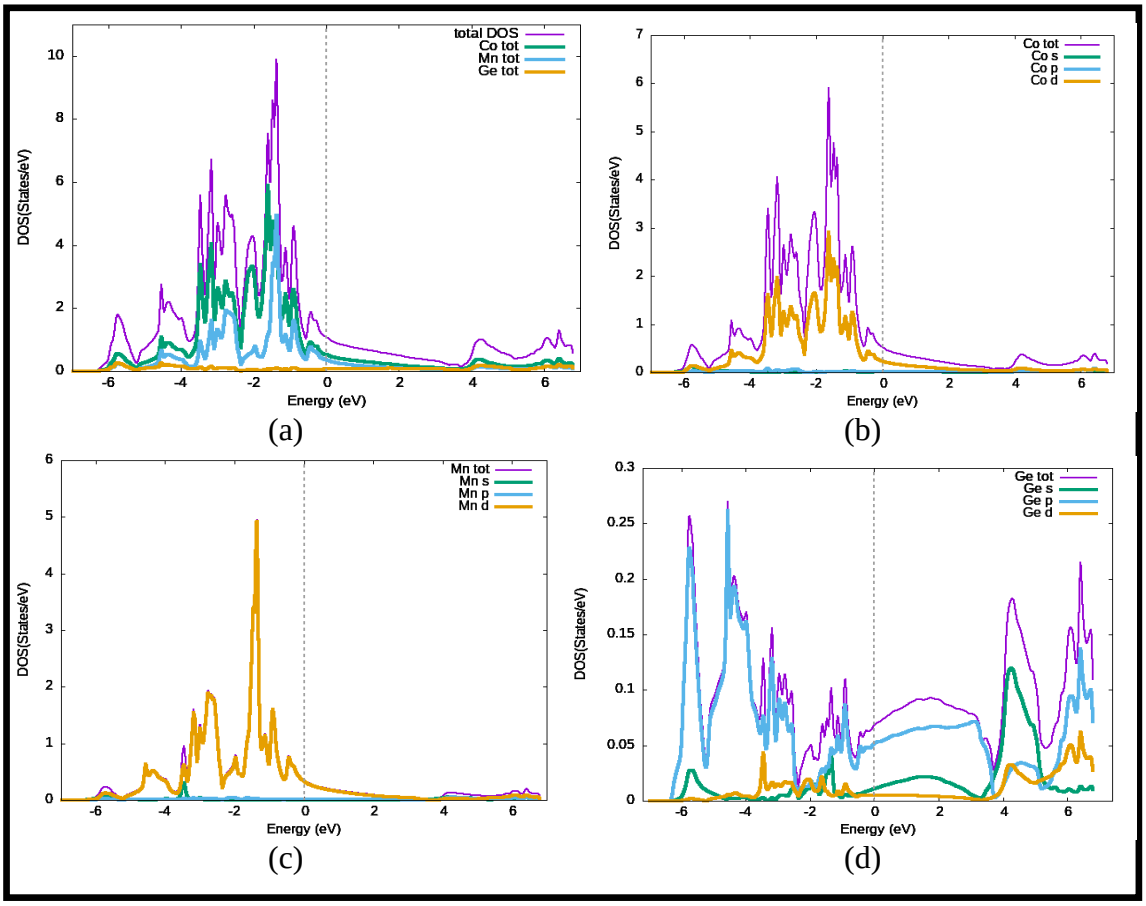

Note: (a) TDOS (b) PDOS for Co atom, (c) PDOS for Mn atom, (d) PDOS for Ge atom.

Figure 24

TDOS and PDOS of spin-down for normal Co_2MnGe compound using mBJ

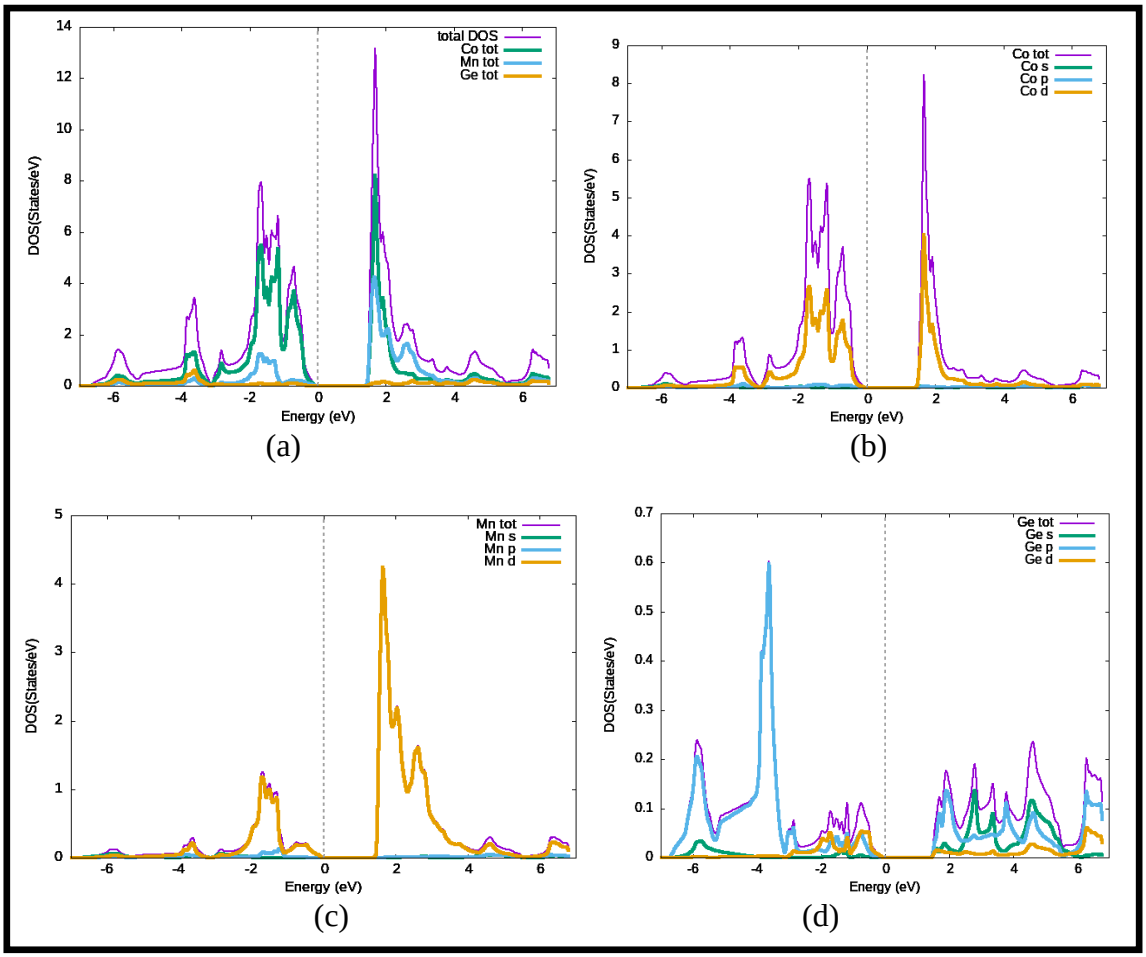

Note: (a) TDOS (b) PDOS for Co atom, (c) PDOS for Mn atom, (d) PDOS for Ge atom.

Figure 25

TDOS and PDOS of spin-up for inverse Co_2MnGe compound using mBJ

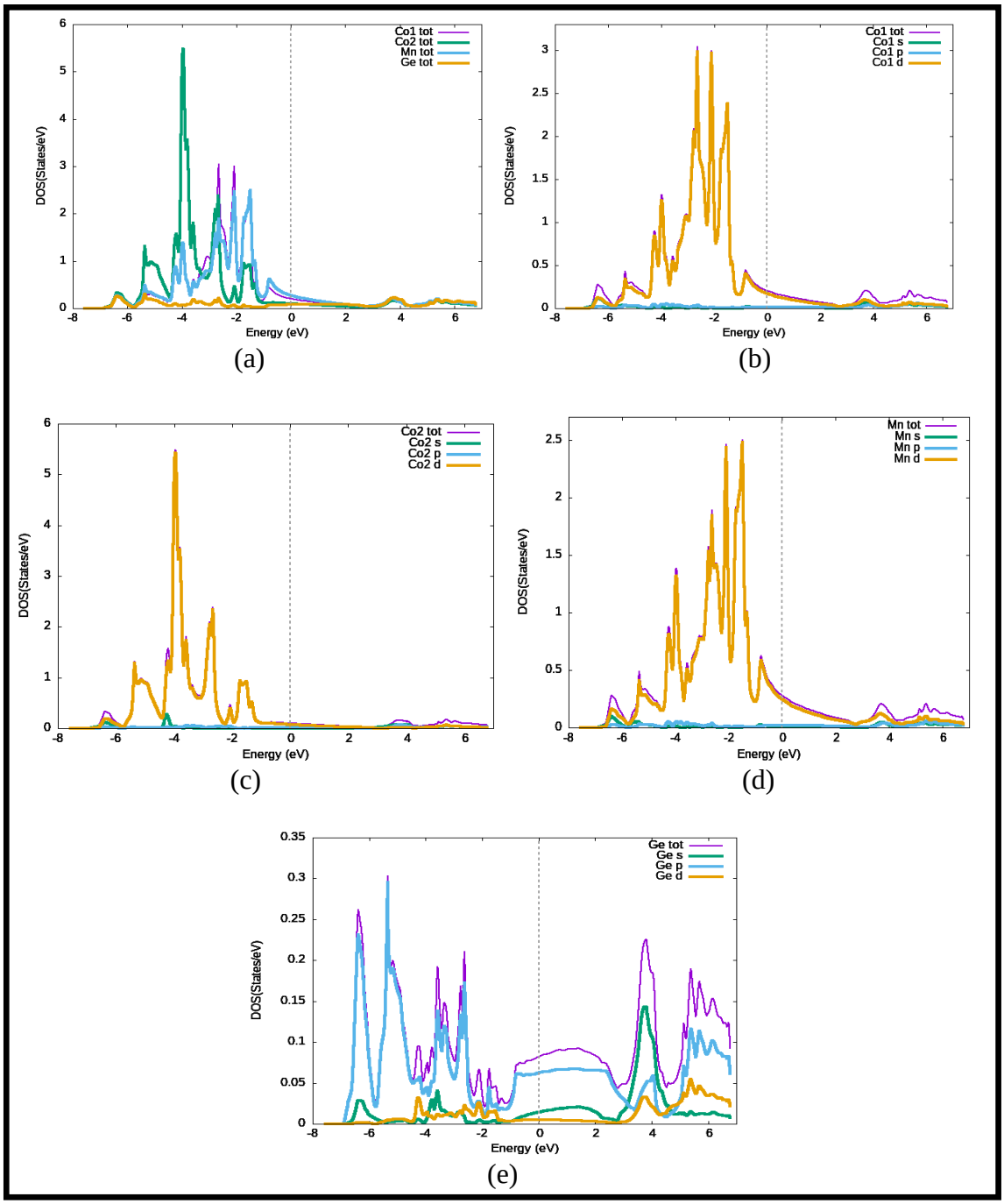

Note: (a) TDOS (b) PDOS for Co_1 atom, (c) PDOS for Co_2 atom, (d) PDOS for Mn atom, (e) PDOS for Ge atom.

Figure 26

TDOS and PDOS of spin-down for inverse Co_2MnGe compound using mBJ

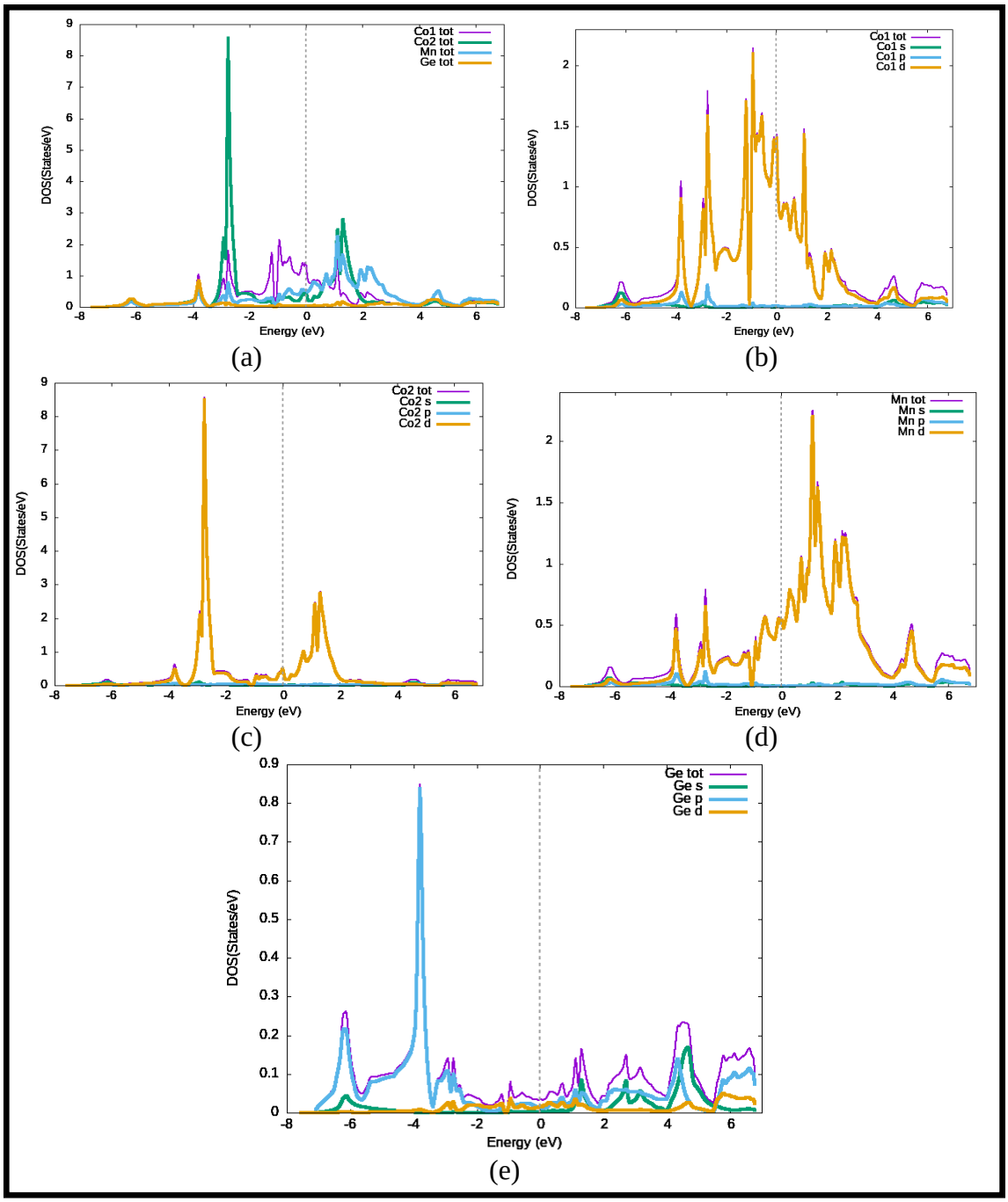

Note: (a) TDOS (b) PDOS for Co_1 atom, (c) PDOS for Co_2 atom, (d) PDOS for Mn atom, (e) PDOS for Ge atom.

جامعة النجاح الوطنية
كلية الدراسات العليا

الخصائص التركيبية، الإلكترونية، المغناطيسية والمرونية لمركبات هيزلر التامة (Co_2MnGe، Co_2MnSi) باستخدام طريقة الجهد التام

إعداد
دعاء علي محمد حسن

إشراف
د. محمود فاروط
أ. د. محمد أبو جعفر

قدمت هذه الرسالة استكمالا لمتطلبات الحصول على درجة الماجستير في الفيزياء،
من كلية الدراسات العليا، في جامعة النجاح الوطنية، نابلس – فلسطين.

2025

الخصائص التركيبية، الإلكترونية، المغناطيسية والمرونية لمركبات هيزلر التامة (Co_2MnGe، Co_2MnSi) باستخدام طريقة الجهد التام

إعداد

دعاء علي محمد حسن

إشراف

د. محمود فاروط

أ. د. محمد أبو جعفر

الملخص

تم دراسة الخصائص التركيبية، الإلكترونية، المغناطيسية و المرونية لمركبات هيزلر التامة (Co_2MnSi و Co_2MnGe) الطبيعية و العكسية باستخدام طريقة الجهد التام (FP-LAPW) ضمن نظرية الكثافة الوظيفية (DFT) وذلك باستخدام حزمة برنامج WEIN2K. تم استخدام تقريب التدرج المعمم (GGA) لدراسة الخصائص التركيبية مثل معامل الشبكة (a)، معامل الكتلة (B)، مشتقتها الأولى للضغط (B')، والحد الأدنى للطاقة (E_0). بالإضافة إلى تقريب التدرج المعمم (GGA)، تم استخدام تقريب بيكي–جونسون المعدل (mBJ) لتحسين فجوة الطاقة المحسوبة (BS). وفقاً لفجوات الطاقة (BS) و كثافة الحالة (DOS) فإن مركبات هيزلر (Co_2MnSi و Co_2MnGe) الطبيعية مركبات نصف معدنية، بينما مركبات هيزلر (Co_2MnSi و Co_2MnGe) العكسية مركبات معدنية. كما تبين أن كلاً من مركبات هيزلر (Co_2MnSi و Co_2MnGe) الطبيعية و العكسية هي مركبات فرومغناطيسية. مركبات هيزلر (Co_2MnSi و Co_2MnGe) الطبيعية ومركب هيزلر (Co_2MnSi) العكسي مستقرة ميكانيكياً، بينما مركب هيزلر (Co_2MnGe) العكسي غير مستقر ميكانيكياً. بالنسبة إلى معامل تباين الخواص (A) فإن مركبيّ هيزلر (Co_2MnSi) الطبيعي والعكسي ومركب هيزلر (Co_2MnGe) الطبيعي مواد متباينة الخواص مرونياً. نسبة باغ (B/S) تبين أن مركبيّ هيزلر (Co_2MnSi) الطبيعي والعكسي و مركب هيزلر (Co_2MnGe) الطبيعي جميعها مركبات مرنة. وفقاً

لنسبة بويزون (**v**) فإن مركبيّ هيزلر (Co_2MnSi) الطبيعي والعكسي ومركب هيزلـــر (Co_2MnGe) الطبيعي جميعها تمتلك روابط أيونية.

الكلمات المفتاحية: مركبات هيزلر، خواص تركيبية، إلكترونية، مغناطيسية، مرونية.